The Pennsylvania State University

The Graduate School

College of the Liberal Arts

FUNCTIONAL NETWORK CONNECTIVITY WITHIN POSTEROLATERAL PARIETAL CORTEX AND ITS ALTERATION IN TRAUMATIC BRAIN INJURY

A Dissertation in

Psychology

by

Umesh Meyyappan Venkatesan

Submitted in Partial Fulfillment
of the Requirements
for the Degree of

Doctor of Philosophy

December 2017

The dissertation of Umesh M. Venkatesan was reviewed and approved* by the following:

Frank G. Hillary
Associate Professor of Psychology
Dissertation Adviser
Chair of Committee

Nancy A. Dennis
Associate Professor of Psychology

Stephen J. Wilson
Associate Professor of Psychology

Charles Geier
Associate Professor of Human Development and Family Studies

Melvin Mark
Department Head and Professor of Psychology

*Signatures are on file in the Graduate School.

ABSTRACT

Spatially distributed functional brain networks show multiple points of regional convergence (“hubs”), suggesting that local network architecture supports global systems communication. Traumatic brain injury (TBI) alters global connectivity patterns, but relatively little is known about its effect on interactions within local hub environments and whether this has implications for cognition. The goal of the dissertation was to examine one such environment, the posterolateral parietal cortex (PPC), in relation to distributed network connectivity and cognition in both TBI (n=18) and healthy controls (n=19). Using resting-state functional MRI in conjunction with seed-voxel and graph theoretical connectivity analyses, the study revealed evidence for increased connectivity, or hyperconnectivity, in TBI from portions of left and right PPC to right-lateralized default mode and frontoparietal control network regions, as well as within the local right PPC network itself. Across groups, right versus left PPC showed increased local connection strength and decreased betweenness centrality, a measure of network hubness. In TBI, strength and global efficiency within the right PPC were strongly negatively correlated with auditory attention span and attentional reaction time, respectively. Overall, these findings substantiate hyperconnectivity on both global and local levels after TBI. Importantly, they propose a special role for local network communication within the right hemisphere in facilitating large-scale information transfer after neurologic insult. Local network organization in TBI also appears to have consequences for cognitive functioning, potentially reflecting a need to balance functional resource demand with network efficiency.

TABLE OF CONTENTS

List of Tables

List of Figures

Acknowledgements

I express my gratitude to my academic adviser, Dr. Frank Hillary, for investing in my scholarship and providing me with the tools and resources necessary for a successful graduate career. I also extend thanks to my academic family at Penn State, including my “labbies”, whose support has been critical to my professional and personal development.

I am indebted to my parents, Swarna and Venkat Venkatesan, for their consistent support in myriad ways and their unconditional love throughout all my endeavors.

Finally, I would like to thank our research participants, especially those living with traumatic brain injury, for their time and dedication to the current work.

Chapter 1. Background and Significance

Overview and Statement of the Problem:

Previous functional connectivity studies have either captured the functional organization of distributed brain networks or investigated whole-brain connectivity patterns associated with individual regions. Although canonical functional networks can be studied via either approach, they do not consider subtle shifts in network dynamics that may occur within the local neural milieu of defined anatomic regions, such as those that exhibit significant functional heterogeneity. Essentially, this is an issue of granularity, and refers to the idea that current research may not be addressing brain-behavior relationships at the highest resolution. Furthermore, previous whole-brain connectivity data suggest that the brain can be characterized by both properties of a small-world and scale-free organization (van den Heuvel, Stam, Boersma, & Hulshoff Pol, 2008); in particular, small-world networks consist of a few critical connections between remote network nodes to allow for information transfer between brain systems, but higher local connectivity (clustering) around individual nodes (Bassett & Bullmore, 2006), which are thought to be responsible for the ability of the nodes to flexibly engage or disengage with the larger brain infrastructure (Hellyer, Scott, Shanahan, Sharp, & Leech, 2015). In order to capture the latter, which reflects the microscale dynamics of the brain, it is necessary to delineate the functional connectivity patterns (or "architecture") within the local environment of individual nodes. In doing so, we may achieve a better understanding of functional organization in typical brain functioning, as well as the impact of local neuroplasticity on behavior after diffuse neurologic disruption.

Rationale and Principal Questions:

Over the past decade, functional neuroimaging has undergone a paradigm shift from examining signal activation of distinct regions to exploring the functional and anatomical architecture of the brain. This line of research has evolved rapidly with increasing recognition of the importance of distributed brain systems in cognition and behavior, and a concurrent emphasis on intrinsic brain activity as revealed by the resting state (resting-state functional connectivity, or RSFC) (Biswal, Yetkin, Haughton, & Hyde, 1995). Aside from revealing the elegant computational architecture of the human brain, network neuroscience has provided a parsimonious framework in which disparate cognitive processes can be subsumed in an integrated, rather than modular, model of brain functioning. For example, the now famous “default mode” network was first defined by Raichle 15 years ago (Raichle et al., 2001); since this time, other putative functional networks, attributed to various cognitive states (Shirer, Ryali, Rykhlevskaia, Menon, & Greicius, 2012; Spreng, Stevens, Chamberlain, Gilmore, & Schacter, 2010), have been shown to participate in complex reciprocal relationships with the DN and each other. While there is some variability between studies regarding the constituent regions (nodes) of intrinsic networks, a discrete set of regions do demonstrate consistent network affiliations.

Whole-brain connectivity techniques have identified a set of intrinsic functional “hub” regions in the brain (Buckner et al., 2009; Power, Schlaggar, Lessov-Schlaggar, & Petersen, 2013; Tomasi & Volkow, 2010). At a fundamental level, hubs refer to regions that maintain a relatively greater number of functional connections to other regions of the brain, and therefore can be thought of as nodes important for integrating and

negotiating between different types of neural information. Consequently, hubs are often regarded as heteromodal, and are thought to comprise functionally heterogeneous subregions that communicate with each other to facilitate whole-brain network negotiation (for an example in the posterior cingulate, see (Leech, Braga, & Sharp, 2012; Leech, Kamourieh, Beckmann, & Sharp, 2011). In the set of whole-brain functional hubs, a commonly implicated region is the posterior parietal cortex (PPC); in its more inferior reaches, the focus of the current investigation, this region comprises the inferior parietal lobule (IPL) and adjacent intraparietal sulcus (IPS). The PPC has a long history in functional neuroimaging research, which has shown that it activates during a variety of cognitive tasks and states. Not surprisingly, functional connectivity work has also shown that there exists an especially striking pattern of functional heterogeneity across PPC subregions that can be linked to previously defined functional systems, such as the default and salience networks (Uddin et al., 2010; Liang, Wang, Yang, & Li, 2012; Zhang & Li, 2014). However, while its participation in diverse networks has been established, virtually nothing is known about how the PPC's subdivisions are directly related to behavior, perhaps due to the fact that previous literature on the topic is in healthy individuals with limited behavioral variability. Furthermore, it is unclear how the PPC *integrates* information from multiple, distinct functional systems. Although it is reasonable to conclude that functionally distinct subregions of the PPC must communicate with each other, little is known about how this occurs. To date, no studies have examined the local network structure of the PPC, which may reveal important information about its functional heterogeneity and that can help clarify its role in behavior, and importantly, inform us about how information

transfer and integration occurs between distinct functional networks subserving behavior. The characterization of the PPC's local (intra-PPC connections) functional properties, especially as they relate to behavior in healthy and pathological brain functioning, is the foci of this proposal.

As a cortical hub, the PPC is thought to exert greater influence than other nodes on distributed brain systems. Therefore, it is interesting to examine the consequences of its disruption on brain function and behavior. This information, in turn, may reveal important functional properties of the PPC and bring us closer to characterizing its specific roles in behavior. To this end, it has been suggested that the study of cortical hubs utilize lesion models, which can reveal unique information about a hub's importance in a larger context (Power et al., 2013). However, such models are difficult to construct for the human PPC, as selective injury to this location is seldom observed. For example, in neurodegenerative diseases where lateral parietal atrophy may be seen, there is also gray matter destruction of other cortical hubs, precluding any specific inferences about PPC function as well as limiting the basic neural resources available for network participation and communication (Hillary et al., 2015).

A clinical disorder appropriate for specifically investigating the PPC is traumatic brain injury (TBI). Here, diffuse white matter (axonal) pathology results in disrupted neuronal communication, with relatively spared neuronal cell bodies (Filley, 2011). While the pathophysiology of TBI does not represent a lesion model of the PPC, it nonetheless lends itself to study of this region's local functional architecture for two primary reasons. The first concerns the pathophysiology of head trauma. TBI has traditionally been considered a disorder of the frontal lobes, and the frontal cortex is

especially vulnerable to the mechanics of injury (McAllister, 2008). Accordingly, studies of TBI have historically focused on frontal lobe neuropathology. However, more recent literature has demonstrated that while structural damage may not predominate in posterior cortical areas in TBI, there are empirical changes in functional synchronization throughout the brain— including major posterior hubs— that have implications for behavior (Bonnelle et al., 2011; Sharp et al., 2011; Venkatesan, Dennis, & Hillary, 2015). These findings suggest that structural disruptions to more frontally based structures are reflected in posterior cortical systems, particularly in posterior cortical hubs (see Hillary & Grafman, 2017), and there exists direct evidence for this structural-functional relationship in TBI (Bonnelle et al., 2012). Thus, even in the absence of frank structural damage to the PPC, connectivity patterns within it may be altered after traumatic insult, offering an opportunity to examine how its local connections are relevant to behavior.

A second advantage of a TBI model pertains to the clinical manifestation of head injury and its relationship to the PPC's functional heterogeneity. The symptomatology of TBI maps on well to the major neural networks currently identified for different types of cognition, such as "goal-directed" and "self-referential" mental processes. For example, goal-directed cognitive deficits in TBI (executive functioning and inhibitory control, working memory, attention, and information processing speed) are among the most consistently reported post-traumatic symptoms (Mattson & Levin, 1990; McAllister, 2011; McDonald, Flashman, & Saykin, 2002). On the other hand, psychiatric and social cognitive impairments, which are often associated with deficits in introspective, self-referential thinking, are also common and persistent TBI sequelae (Bombardier et al.,

2010; Dikmen, Bombardier, Machamer, Fann, & Temkin, 2004; Hoofien, Gilboa, Vakil, & Donovick, 2001; Koponen et al., 2002; Rapoport, 2012). Overall, these clinical features indicate that TBI results in simultaneous disruptions to multiple, discrete cortical systems which, incidentally, are well represented in the functional connectivity patterns of PPC subregions. Moreover, there is functional neuroimaging evidence to suggest that cognitive deficits in TBI reflect a reduced ability to inhibit and/or efficiently "switch" between cortical systems (Bonnelle et al., 2012). Here, the potential identification of a local hub (or hubs) in the PPC has special significance for TBI. Addressing whether injury results in the disruption of these hubs would facilitate inferences about the relationship between network communication/integration within the PPC and complex behavioral processes requiring the coordination of multiple brain systems (e.g., switching between internally- and externally-directed cognitive states).

As in previous studies of intrinsic connectivity, the current work targets the rapidly shifting patterns of synchrony and asynchrony in the brain. However, it aims to expand on what is known about the connectivity patterns of a functionally heterogeneous region, the PPC, which is positioned at the crossroads of several distinct functional networks. The current study first investigates the PPC's relationship to whole-brain networks to confirm and expand upon previous reports of functional heterogeneity within this region, probing changes in this organizational heterogeneity in TBI. The study then examines the region's local functional architecture as a single graph, or network, incorporating interrelationships between subregions defined in a data-driven manner. The goal here is to determine the quality of neuroplastic changes in functional connection strength, importance, and integration within the PPC network after TBI. At

the third level, the study aims to delineate relationships between these graph theoretical properties of the PPC network and behavior.

Chapter 2. Structure and Function of PPC, Relationship to Functional Networks, and Relevance to TBI (literature review)

This chapter provide an overview of the structure of the PPC and its known functional properties to illustrate the importance of examining local functional architecture in understanding both normal and pathological brain functioning. The structure of the PPC and its theorized roles in behavior are reviewed briefly in the first section. Subsequently, the author discusses literature on the topology of cognitive networks, especially as they relate to PPC subdivisions and behavior. In the third section, the reader is presented with an overview of TBI, where the delineation of the PPC's local functional properties may be important in understanding the relationship between network disruption and cognitive deficit, and can, in turn, inform cognitive neuroscientific models of integrated brain function.

Part I: Structure and Function of the Posterolateral Parietal Cortex

The PPC encompasses a readily identifiable area of cortex restricted to the lateral parietal lobe. It consists of three distinct macro-anatomic landmarks, including the supramarginal gyrus (Brodmann area 40) and angular gyrus (Brodmann area 39), both of which form the inferior parietal lobule, as well as the intraparietal sulcus, which lies immediately superior to these gyri. Anatomic parcellation studies of the PPC have examined the cytoarchitectonics of this region. Cytoarchitecture refers to the microscopic cellular composition of brain tissue, or how neuronal bodies are layered within a certain brain area. Performed by von Economo and Koskinas in 1925 (Triarhou, 2007) as part of whole-brain partitioning, the original parcellation of the PPC revealed

multiple cytoarchitectonic subtypes in the IPL, though the extent to which they constituted unique subdivisions requiring separate classification was unclear. In contrast, the IPS remained unitary.

Much later, Caspers and colleagues (Caspers et al., 2006; Caspers et al., 2008) offered a more detailed cytoarchitectonic parcellation of the IPL in the human brain involving 10 distinct subdivisions in each hemisphere: the more anteriorly positioned PFop, PFt, PFcm, PF, and PFm, and the more posteriorly oriented PGa and PGp. These subregions have been shown to exhibit differential neurotransmitter receptor structures, suggesting not only anatomic but also molecular segregation within the IPL (Caspers et al., 2013). In the human intraparietal sulcus, three major subdivisions have been defined, and from anterior to posterior they are: hIP1 and hIP2 (Choi et al., 2006), and hIP3 (Scheperjans et al., 2008). Importantly, contemporary anatomic parcellation schemes of both the IPL and IPS can be identified with anatomic homologues in monkeys (Gregoriou, Borra, Matelli, & Luppino, 2006; Pandya & Seltzer, 1982; Scheperjans et al., 2008).

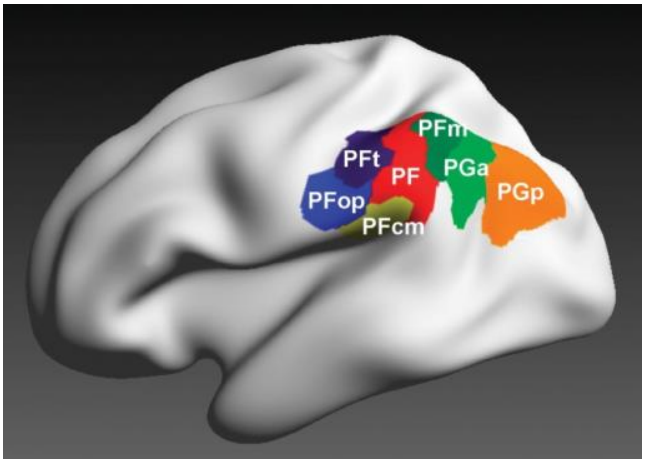

As might be expected, the structural connectivity of the PPC differs across its subregions. For example, fiber tracking using diffusion tensor imaging (DTI) has revealed that anterior IPL (“PF-” regions) primarily maintains anatomic connections with inferior frontal, motor, premotor, and somatosensory areas, whereas posterior IPL (PGa, PGp) is more strongly linked with posterior (medial) parietal, higher visual, and temporal areas (Caspers et al., 2011; Uddin et al., 2010). A similar anterior to posterior shift in structural connectivity has been observed in the IPS, with anterior areas exhibiting robust connections to the frontal lobes and operculum, and posterior areas most strongly connected to occipital cortex (Bray, Almas, Arnold, Iaria, & MacQueen, 2015; Uddin et al., 2010).

Likely due to its structural connections with a breadth of cortical regions, the PPC has been implicated a wide variety of cognitive functions. While an exhaustive review is beyond the scope of this discussion, it is important to take note of the vast functional neuroimaging literature that has demonstrated the PPC’s involvement in tasks of episodic and working memory (Berryhill, 2012), executive functioning (Niendam et al., 2012), and bottom-up attentional processes, particularly as applied to memory retrieval (Behrmann, Geng, & Shomstein, 2004; Cabeza, Ciaramelli, Olson, & Moscovitch, 2008; Corbetta & Shulman, 2002; Corbetta, Patel, & Shulman, 2008; Hutchinson, Uncapher, & Wagner, 2009; Shomstein, 2012). In fact, the angular gyrus alone is associated with diverse functions from spatial processing to social cognition (Seghier, 2013). Previous work therefore suggests that the PPC is involved in fundamental processes subserving multiple cognitive functions or that it integrates information from divergent cortical systems, or both. Despite the enormous body of research it has stimulated, however,

the PPC still remains somewhat of a mystery with respect to its distinct functional and anatomic components and their interrelations.

Part II: The PPC and Functional Brain Networks

Intrinsic neural networks have traditionally been identified using resting-state functional connectivity analysis, which refers to temporal correlations between low frequency fluctuations of the BOLD fMRI signal in spatially remote brain regions (Friston, Frith, Fletcher, Liddle, & Frackowiak, 1996). While the concept of functional brain signatures is generally accepted as valid, various networks have been identified in the functional connectivity literature. Network definitions across studies often overlap in their spatial coverage, limiting the generalizability of findings in any particular study. Nonetheless, some of the PPC's elusiveness with regard to its association with cognition has been lessened by functional connectivity studies, which have revealed affiliations between its subregions and whole-brain networks that can be classified into three major patterns: connectivity between posterior PPC and regions of the DMN, between the superior PPC and regions of the DAN, and between the anterior PPC and regions of the FCN. Thus, these three networks offer a useful starting point for investigating how network information may be represented and exchanged between PPC subdivisions.

Default Mode Network (DMN)

Among PPC subregions, those corresponding to the angular gyrus demonstrate robust functional connectivity with a set of regions comprising the default mode network (Vincent, Kahn, Snyder, Raichle, & Buckner, 2008). The DMN comprises highly

correlated, spatially distinct brain regions (Greicius, Krasnow, Reiss, & Menon, 2003; Gusnard & Raichle, 2001; Raichle et al., 2001; Raichle & Snyder, 2007) that exhibit greater neuronal activity during passive rest than when performing a cognitively effortful task (Fox et al., 2005; Greicius et al., 2003). Uddin and others (Uddin et al., 2010) examined functional and structural connectivity of the angular gyrus and IPS subregions using resting-state fMRI and the most current cytoarchitectonic definitions mentioned above. They noted that the posterior angular gyrus subregion, PGp, maintained strong functional connectivity to the canonical DMN, including portions of the medial temporal lobe, while PGa was functionally linked to the basal ganglia, ventral premotor areas, and ventrolateral prefrontal cortex. However, studies that have not distinguished between angular gyrus divisions have also found support for its involvement in the DMN (Greicius et al., 2003; Liang et al., 2012; Seghier, 2013). Thus, the posterior lateral parietal cortex, and specifically the angular gyrus, is implicated in most definitions of the DMN, which additionally includes the posterior cingulate, medial prefrontal, and parahippocampal regions as its primary components (Fox et al., 2005; Raichle et al., 2001).

The DMN has been referred to as a task-anticorrelated, or “task-negative”, network that is distinct from a “task-positive” network containing regions commonly activated during a variety of cognitive tasks (Fox et al., 2005). However, due to the increasing recognition of DMN involvement in active cognition, this semantic distinction recently has been challenged (Spreng, 2012). For example, default regions overlap significantly with cortical areas implicated in episodic memory functioning (Buckner, Andrews-Hanna, & Schacter, 2008; Buckner et al., 2005), and as reviewed earlier, the

PPC reflects one of these critical overlaps. The concordance between the memory literature and mounting DMN studies has led investigators to theorize about the roles of the DMN in memory and other cognitive functions, primarily those of self-referential processing and introspective thinking (Buckner et al., 2008).

There is evidence to show that while the DMN can generally be conceptualized as one intrinsic system, there appears to be significant variability in how its member regions are involved in cognition. Recently, Andrews-Hanna and colleagues (Andrews-Hanna, Reidler, Sepulcre, Poulin, & Buckner, 2010) performed a functional parcellation of the DMN, from which they identified: a midline core consisting of the anterior medial prefrontal cortex and posterior cingulate cortex; a dorsal medial prefrontal subsystem incorporating the dorsal medial prefrontal cortex, temporoparietal junction, lateral temporal cortex and temporal pole; and a medial temporal subsystem including the ventral medial prefrontal cortex, posterior inferior parietal lobule, retrosplenial cortex, parahippocampal cortex, and hippocampal formation. Interestingly, they observed that these systems could be dissociated based on the type of mental activity in which they were principally involved. While the dorsal medial prefrontal system was more active during tasks requiring thinking about the self in the present, the medial temporal system showed preferential activation during judgments about the self in some future time, suggesting a role for this system in using memory to construct mental representations/ simulations of the self in the future. As expected, the core subsystem was comparably active in both types of self-referential thinking. These findings find further support in a subsequent meta-analysis that revealed neural dissociations between episodic memory and mentalization ability, with both mental processes subserving autobiographical

memory (Andrews-Hanna, Saxe, & Yarkoni, 2014). Hence, the DMN appears to comprise multiple related components that are often simultaneously engaged during complex, internally directed thinking, but its dynamic activity is not limited to member regions. Another indication that the DMN is heterogeneous system is that it couples and decouples flexibly with regions of other brain systems (Uddin, Kelly, Biswal, Castellanos, & Milham, 2009). However, little is known about the mechanisms behind this chameleonic feature.

Dorsal Attention Network (DAN)

More superior regions of the PPC, components of the IPS, exhibit strong connectivity with the superior parietal lobule, MT+ area, and frontal eye field (FEFs) (Vincent et al., 2008; Vinette & Bray, 2015). Uddin and colleagues (2010) also demonstrated that IPS subregions hIP1 and hIP2 were both correlated with signals in the frontal cortex, with hIP1 additionally being connected to the insula, while hIP3 maintained connectivity to visual areas. Contrasted with evidence for PPC-DMN connectivity, these findings reflect PPC connectivity to a group of regions collectively known as the dorsal attention network, which can be thought of as the functional antithesis of the DMN.

The DAN has its origins in the seminal work of Corbetta and Shulman (2002), who proposed that goal-directed cognition (i.e., cognition directed by or towards external stimuli) was supported by two distinct but interrelated frontoparietal systems, the dorsal and ventral attention networks. They argued that while a dorsal stream in the brain is responsible for top-down control of behavior (attentional allocation), a ventral

stream is engaged to orient attention to novel or salient stimuli (attentional shifting). In rudimentary terms, they considered the dorsal system to be voluntary, while the ventral system is largely reflexive. While a simplistic dual-attention model is often eschewed today, it still has heuristic value and finds support in more recent neuroimaging literature (Vossel, Geng, & Fink, 2014). The notion of a dorsal attentional stream is continued in the contemporary DAN, which, as in Corbetta and Shulman's original definition, principally includes bilateral FEFs and, not surprisingly, the IPS (Fox, Corbetta, Snyder, Vincent, & Raichle, 2006). Some studies have also variously included portions of the superior parietal lobule (SPL), inferior precentral sulcus, superior occipital gyrus, and middle temporal motion complex (MT+) in their delineation of the DAN (Fox et al., 2005; Spreng, Sepulcre, Turner, Stevens, & Schacter, 2013; Szczepanski, Pinsk, Douglas, Kastner, & Saalmann, 2013; Vincent et al., 2008).

Whereas there is evidence to show that the DAN is involved in attentional control across modalities (Macaluso, 2010), it has been most comprehensively studied in the context of visuospatial attention. Previous studies have demonstrated that both the FEFs and IPS contain retinotopic maps of the contralateral visual field, suggesting a critical role in a number of visually-mediated cognitive tasks, including visual working memory (Jerde, Merriam, Riggall, Hedges, & Curtis, 2012). Furthermore, effective connectivity and TMS studies during task performance have noted a causal influence of these regions on visual areas in occipital cortex (Vossel et al., 2014), lending more credence to the idea of the DAN as a (primarily visual) attentional control system. However, the DAN also constitutes a unique functional signature in the resting brain, and a study in healthy individuals represents the first empirical evidence of the DAN's

intrinsic presence (Fox et al., 2006). Using resting-state fMRI and seed-voxel correlations, these researchers identified largely overlapping connectivity maps for their FEF and IPS seeds, suggesting that these regions not only work in functional concert during task, but are also synchronous in the absence of external stimuli.

It is generally agreed that the dissociable DMN and DAN systems communicate in some manner to facilitate complex cognition (i.e., switching between of externally- and internally-directed mental states in accord with environmental or personal demands). Indeed there is ample literature documenting that concurrent modulations of the DMN and "task-positive" (including DAN) support task performance in healthy individuals (Arsalidou, Pascual-Leone, Johnson, Morris, & Taylor, 2013; Hampson, Driesen, Roth, Gore, & Constable, 2010; Kelly, Uddin, Biswal, Castellanos, & Milham, 2008; Weissman, Roberts, Visscher, & Woldorff, 2006). Exactly how this modulation occurs, however, remains unclear. Several studies have made theoretical references to go-between brain systems for information integration, noting shared connectivity patterns with two brain networks. For example, in addition to a dorsal attention system, Fox and colleagues (2006) noted an intrinsic ventral attention network, and found that it overlapped with the DAN in its functional connectivity to portions of the right middle frontal gyrus, inferior frontal gyrus, and inferior parietal lobe. Interestingly, the authors attributed the parietal lobe effect to spatial blurring, but did acknowledge a potential integrative system in the brain for coordinating attentional networks. Since their study, some of these regions of connectivity overlap, including those in posterior parietal lobe, have been identified as part of an apparently distinct network interposed between neural ensembles for goal-directed (DAN) and self-referential (DMN) cognition, and serving to

integrate information from these cognitive modalities. This suggests that in a local connectivity environment such as the PPC, there is a point(s) of convergence between the DAN and DMN that may facilitate neural information transfer and integration.

Frontoparietal Control Network (FCN)

While posterior and superior subregions of the PPC are implicated in the DMN and DAN, respectively, the anterior PPC (supramarginal gyral area) exhibits another distinct connectivity pattern, which only recently has gained attention in network neuroscience. Seed-voxel analyses investigations have revealed functional connectivity between the anterior PPC and a set of distributed regions, including the anterior prefrontal, anterior cingulate, and anterior insular cortices (Vincent et al., 2008) as well as a portion of the precuneus (Spreng et al., 2010). Collectively, these regions appear to constitute a third network— a spatial intermediary between the DMN and DAN— the frontoparietal control network (Vincent et al., 2008).

Until recently, “frontoparietal network” was an umbrella term for networks with constituent regions in the frontal and parietal lobes. With increasing recognition of the brain as a composite of dynamic and overlapping systems, there emerged a need to identify and characterize an integrative component that could unify spatiotemporally disparate neural ensembles to make complex cognitive functioning possible. This gap was first addressed by Vincent and colleagues (2008), who studied resting-state functional connectivity with seed-voxel analyses in healthy individuals and observed three distinct brain systems: a hippocampal-cortical memory network (reflecting a portion of the DMN), a primarily superiorly oriented network corresponding to the DAN,

and a third system anatomically interposed between them, which the authors termed the FCN. This network includes regions typically identified as part of a “salience” network (SN) for attentional orienting (dorsal anterior cingulate and anterior insula) (Menon & Uddin, 2010; Seeley et al., 2007), as well as the anterior prefrontal, dorsolateral prefrontal, dorsomedial superior frontal, and anterior inferior parietal cortices (Vincent et al., 2008).

The existence of a specific intrinsic FCN as defined above has been supported by a recent metanalysis (Niendam et al., 2012). Moreover, the behavioral significance of the FCN has been demonstrated by studies that found preferential engagement of the DMN and DAN during autobiographical and visuospatial planning, respectively, but FCN activity during both types of planning behavior in healthy adults (Spreng & Schacter, 2012; Spreng et al., 2010). Hence, the FCN appears to operate as an executive control system that is not only involved in goal directed cognition, but enables flexible negotiation between neural substrates for externally and internally directed cognition. Further supporting this role for the FCN is graph theoretical evidence from whole-brain resting-state data, which has demonstrated that while integrated in a distinct network, individual nodes of the FCN show functional affinities with either the DMN or DAN, or both (Spreng et al., 2013).

Taken together with the DAN and DMN, the FCN may complete a unique triad of neural systems integral to mentation, with its purpose being the efficient negotiation of information between cognitive systems. Importantly, the representation of all three of these networks in the connectivity patterns of PPC subregions suggests that their interactions run deep, that is, not only at the broader whole-brain level but also within

the local topology. Here, the critical question of how information transfer is achieved between the network triad in the PPC remains unanswered, and if clarified, may ultimately reveal properties of functional organization that underlie complex behavioral processes and permit shifting between them.

Part III: Traumatic Brain Injury and Network Disruption

Brain injuries can be classified along a large spectrum of severity, which can be defined by level of consciousness/responsiveness, commonly assessed by the Glasgow Coma Scale (GCS) (Teasdale & Jennett, 1974), loss of consciousness (LOC) duration, and the duration of post-traumatic amnesia (PTA), a temporary state of confusion and disorientation following trauma. The current discussion focuses on moderate to severe forms of non-penetrating (i.e., closed-head) brain injury, which are distinguished from milder injury such as concussion, and typically involve a prolonged PTA or loss of consciousness, and/or abnormalities on structural neuroimaging.

Among the most common features of moderate to severe brain injuries are cerebral contusions, hemorrhages, and diffuse or traumatic axonal injury (DAI/TAI) (Maas, Stocchetti, & Bullock, 2008); these abnormalities may occur in isolation, but are frequently concurrent in more severe forms of injury. While contusions and hemorrhages are usually due to impact of the head with a foreign body, and thus constitute focal injuries, DAI involves the mechanistic stretching and subsequent degeneration of neuronal axons in several areas, resulting from rapid accelerative-decelerative and/or rotational forces on the brain (Gennarelli & Graham, 1998; McIntosh et al., 1996). Because diffuse axonal damage impairs neural communication, TBI is

viewed as a disorder of disrupted neural networks (Hayes, Bigler, & Verfaellie, 2016). Therefore, TBI serves as an important model for studying the influence of network connectivity patterns on behavior, and its promise in this regard is already emerging (e.g., Bonnelle et al., 2012; Bonnelle et al., 2011; Hellyer et al., 2015).

Investigation of functional network connectivity in TBI has prominently featured the DMN along with regions commonly implicated in externally directed cognition. Kim and colleagues (2010) were the first to report on resting-state perturbations in TBI. They measured absolute cerebral blood flow (CBF) in individuals with moderate to severe injuries, and found reductions, compared to controls, most notably in bilateral PCC, bilateral thalamus, and more rostral areas such as bilateral anterior cingulate and middle frontal cortices. In TBI, relative hypoperfusion was also seen in posterior cingulate and thalami, but there was evidence of relative hyperperfusion in right temporal gyri and the insula. Although no neuropsychological data were presented, hypoperfusion in DMN regions was thought to be related to cognitive impairment. Subsequently, in an analysis of “rest” intervals from a working memory task, another study observed a shift in network dynamics during injury recovery (from 3-6 months post-injury), consisting of increased connectivity within the DMN but decreased connectivity in a “goal-directed” network consisting of anterior cingulate and dorsolaterial prefrontal cortices (Hillary et al., 2011). Accompanying these changes was a longitudinal increase in connectivity from both default and goal-directed regions to the insula, a SN region. Again, results suggested that clinical recovery from TBI was subserved by dynamic changes within and between distributed neural networks, although the relation of these network changes to behavior remained unclear.

Other studies exploring neural network connectivity in TBI have reported increased within-DMN functional connectivity, featuring prominently the PCC and precuneus regions, using ICA and dual regression techniques (Bonnelle et al., 2011; Sharp et al., 2011). These investigations have attempted to elucidate the relationship between functional network connectivity and task performance. For example, Sharp et al. (2011) noted greater connectivity of the posterior cingulate to the rest of the DMN in TBI relative to healthy participants. Because faster reaction times were associated with greater connectivity in the patient sample, an adaptive, or compensatory, role for this increased connectivity was proposed. In a separate investigation from the same group, functional connectivity of precuneus to remaining DMN at the beginning of a choice reaction time (CRT) task was negatively associated with change in reaction time (RT) during that task, suggesting that higher connectivity supports better and more stable performance (Bonnelle et al., 2011). These authors also found that the magnitude of precuneus-DMN connectivity correctly classified a subgroup of individuals with TBI demonstrating deficits in sustained attention compared to both controls and brain-injured individuals with intact sustained attention. However, as the low-sustained attention TBI group was defined based on greater increase in RT between time-points, it is unclear whether what the authors referred to as a “vigilance decrement” is truly attention-related or an artifact of cognitive fatigue. Moreover, neither of the two immediately aforementioned studies examined relationships between DMN and regions of other intrinsic networks.

More recently, TBI connectivity research has shifted focus to networks besides the DMN. One study examined the association of the DMN with the SN during response

inhibition/switching (Jilka et al., 2014), based on previous findings linking the loss of structural integrity in the SN to functional DMN alterations (Bonnelle et al., 2012), and found that the functional connectivity between the anterior insula and DMN is directly impacted by structural breakdown in the SN. It was noted that the SN appears to suppress DMN functioning in the presence of external stimuli requiring attention (Jilka et al., 2014). A previous study from our laboratory examined resting state connectivity in TBI during the subacute (approx. 3 months post-injury) and chronic (approx. 1 year post injury) phases and found evidence for enduring connectivity alterations at the chronic stage involving regions of the DMN, FCN, and SN relative to controls (Venkatesan et al., 2015). Similar longitudinal changes were described by Roy and colleagues (2017), who noted residual hyperconnectivity in both frontal DMN and temporo-parietal attentional control regions at one year post-injury. Furthermore, Hellyer and colleagues (Hellyer et al., 2015) observed that TBI reduces the ability of brain systems at large to flexibly engage and disengage as necessary for behavior. Thus, the incoordination of *multiple* distinct functional networks seems to underlie clinical manifestations of TBI and influence recovery potential.

Overall, empirical observations in the functional connectivity of TBI highlight the importance of dynamic, negotiated activity between neural ensembles. However, investigations of disrupted brain dynamics in TBI have largely been at the whole-brain level. Given increasing evidence of multiple network representations within smaller areas of cortex, it is important to consider the changes in local functional architecture that may be induced by brain injury. The PPC, with its connectivity to major networks implicated in TBI network pathology, offers an appropriate avenue to examine

mechanisms of network communication and integration that have been theorized in previous literature, but remain poorly operationalized. Importantly, the processes of functional communication within the PPC may have significant explanatory power for the cognitive deficits seen in TBI and for individual differences in normal behavior.

Chapter 3. Specific Aims and Hypotheses

Functional connectivity approaches can be employed on both global and local scales. A deeper investigation into the connectivity properties of the PPC utilizing graph theory, an increasingly popular approach to examining complex networks, may help distill and clarify network dynamics not readily discernable in whole-brain analyses. Furthermore, when employed in a clinical model of diffuse axonal pathology, TBI, this approach could add critically to our understanding of distributed brain systems and their interactions, as well as their influence on behavior. The use of head injury as a model for network examination within the PPC is especially interesting given known vulnerabilities of small-world and scale-free networks. These network designs are susceptible to breakdown after targeted “attacks” on hubs (Bullmore & Sporns, 2009), such as those observed for frontal and midline hubs in structural neuroimaging studies of TBI (Fagerholm, Hellyer, Scott, Leech, & Sharp, 2015; Kim et al., 2014). On the other hand, it has been shown that *functional* network disruption in TBI is primarily random, and preserves much of the small-world functional topology of healthy brains (Caeyenberghs et al., 2012; Nakamura, Hillary, & Biswal, 2009), although the strength of the connections in this organization appears to be altered (Nakamura et al., 2009), and research has primarily been at the level of distributed regions. Because TBI represents a unique instance of altered network function in the context of generally intact functional architecture, investigation of this disorder has the potential to shed light on the relationship between the PPC’s intraregional architecture and behavior.

The general goal of the dissertation was to characterize the functional heterogeneity of the PPC, encompassing functional interactions between its

subcomponents and its association with behavior in both intact and disrupted brain systems. To this end, the studies utilized resting-state fMRI and out-of-scanner behavioral data from a sample of healthy individuals and a sample of individuals with moderate to severe TBI (described further in Chapter IV: Methods). Specific aims and hypotheses were as follows:

Aim 1: To identify the correlational relationships between a priori PPC subdivisions and regions of previously characterized intrinsic functional networks, and examine the influence of TBI on this functional architecture. The principal networks of interest are those frequently implicated in cognition, namely, the DMN, DAN, and FCN. Based on previous work and preliminary data from our laboratory, the strength of subregional-whole brain connectivity is expected to be altered in TBI.

Hypotheses:

1. It was predicted that PPC subregions would show increased connectivity, or "hyperconnectivity" to remote regions within their respective networks in TBI as compared to controls. That is, DMN-aligned subregions of the PPC were expected to show stronger functional connectivity with remote DMN regions, and likewise for DAN- and FCN-aligned subregions.

2. It was hypothesized that negative connectivity of DMN-, DAN-, and FCN-aligned subregions with regions outside their respective networks would be increased in TBI relative to controls.

Aim 2: To quantify regional network properties of the PPC in each individual via data-driven parcellation of the local PPC network, or graph. Goals here included, first, characterizing the spatial similarity of parcellations between individuals in each group to examine interindividual variability. If consistent between individuals, group-level adjacency matrices would be constructed, in which examination of hub structure would be possible. If highly variable, group-level matrices to examine hub structure would be eschewed in favor of examining PPC network characteristics on an individual level, and differences in these metrics between groups. The premise for this aim derived from previous observations that the PPC subregions are anatomically juxtaposed and show differential connectivity to whole-brain networks (i.e., regions outside the PPC). In whole-brain data, regions that are at anatomic and functional crossroads (e.g., located in the vicinity of many different functional systems; see, Power et al., 2013) are good candidates for hubs because they are in a privileged position to negotiate information between networks. The same principle can be applied within a region, such as the PPC, whose anatomically proximal and functionally differentiated subregions can themselves be thought to constitute a local network with corresponding network properties that can be evaluated between groups and in relation to behavior (see Aim 3).

Hypotheses:

1. It was predicted that in both groups, the PPC would evidence modular structure, that is, lend itself to parcellation into discrete functional units based on interrelationships between voxel signals.

2a. If modular structure was consistent between individuals: In controls, it was predicted that hubs (those with the greatest degree and betweenness centrality) would be identified in atlas-defined regions connected to the greater FCN in Aim 1. By contrast, in TBI, it was hypothesized that hubs, if substantively present, would occupy positions in subregions aligned with the DMN and DAN.

2b. If modular structure was variable between individuals: It was expected that despite heterogeneity within groups, there would be reduced connectivity strength, nodal influence, and integration (as defined by graph metrics strength, centrality, and global efficiency, respectively) within the PPC network in the TBI group relative to controls. This was conceptualized to reflect potential suboptimal intra-regional information transfer in TBI.

Aim 3: To examine the relationships between PPC connectivity patterns and behavior in each group. In this exploratory analysis, group differences in graph theoretical metrics were targeted for examination with out-of-scanner cognitive variables known to be affected by DAI. These variables comprised scores from traditional neuropsychological tests of attention, processing speed, working memory, and executive functioning, together representing external goal-directed cognition. Additionally, a well-known working memory paradigm was modified to serve as a behavioral analog of switching between externally-directed and internally-directed cognitive processes. an experimental working memory paradigm, modified to serve as an analog of functional network switching, are

used as behavioral indices. Relationships between graph theory metrics and behavior were examined in both control and TBI groups.

Hypotheses:

1. It was hypothesized that across groups, performance on externally-directed (external goal-oriented) neuropsychological tests would be associated with measures of strength, nodal influence, and integration within the PPC.

2. It was predicted that performance on the experimental task requiring switching between externally goal-oriented and self-relevant cognition would be related to network properties of the PPC, and that these relationships would be most robust in TBI due to the behavioral variability resulting from neurologic compromise in this group.

Chapter 4. Procedure and Data Preprocessing

Participants

Participants were recruited as part of ongoing studies within a neuroimaging laboratory at Pennsylvania State University-University Park. In a cross-sectional design, 18 individuals with moderate to severe TBI (ages 20-74; $\bar{x}$ = 41.67, sd = 17.35) and 19 healthy controls (ages 25-79; $\bar{x}$ = 40.74, sd = 14.39) comprised the full study sample. The groups did not differ significantly in mean age or years of education. Distribution of ages, years of education, or gender was not significantly different between groups. TBI severity was defined using the Glasgow Coma Scale (GCS; Teasdale & Jennett, 1974) obtained on admission to the trauma unit. Only individuals with either a GCS score less than 13, loss of consciousness for 30 minutes or more, or with positive neuropathologic findings upon structural neuroimaging were eligible for participation. Individuals with TBI sustained their injury a median of 5.75 years prior to scanning, and time post-injury was not correlated with age (ρ = -0.003, p = 0.990). Candidates for either the TBI group or the HC group were excluded if they had a history of neurologic disorder such as prior TBI, stroke, seizure disorder, or history of serious psychiatric illness (e.g., schizophrenia or bipolar disorder). Individuals were also excluded if they had a history of inpatient treatment for substance abuse. These exclusions were assessed via medical chart review, covered in the institutional review board-approved consent form, and communicated to the study participant and/or the family member(s) of each participant before enrollment. Demographic and clinical characteristics of participant groups are found in Table 1. All research procedures were approved by the Penn State University

Institutional Review Board and all participants provided written informed consent at enrollment. Participants received monetary compensation for their time.

Sample Characteristics				
	TBI	**HC**	**p-value[2]**	**p-value[3]**
Gender	7 M, 11 F	11 M, 8 F	--	0.33
Age	41.67 ± 17.35	40.74 ± 14.39	0.86	0.99
Education	14.22 ± 2.58	13.84 ± 2.48	0.65	0.96
GCS[1]	6.65 ± 3.88	--	--	
Years post-injury	median: 5.75 range: 0.33 – 28.25	--	--	

Table 1. GCS=Glasgow Coma Scale; [1]GCS not available for 2 participants- injury severity was confirmed by loss of consciousness time or positive neuroimaging findings for these individuals; [2]two-sample t-test; [3]non-parametric tests (Mann-Whitney *U* [age, education] or χ^2 [gender]).

Neurocognitive Testing

All participants were administered neuropsychological tests to assess functioning across cognitive domains, with particular focus on attention, processing speed, and executive functioning, given that these are the most vulnerable cognitive abilities in TBI. All participants received a core neuropsychological battery; additional test data were available for a subset of individuals due to general study protocol updates in the laboratory. Cognitive and connectivity (graph theoretical) measures were included in post-hoc exploratory correlations to investigate potential brain-behavior relationships. The approach to these analyses involved balancing the need to minimize statistical comparisons with allowing for examination of PPC graph metrics with a range of cognitive constructs, given its putatively diverse role in cognitive functioning. Therefore, comparisons focused on graph metric(s) that were significantly different between groups and selected cognitive variables theoretically sensitive to the effects of TBI. Descriptive

and inferential statistics for neuropsychological test performances are found in Table 2. Note that although, on average, the TBI group performed worse than the control group on all measures, none of these differences were statistically significant except for RBANS Digit Span.

Neuropsychological Test Performance			
Test	**HC mean (SD); n**	**TBI mean (SD); n**	**Group comparison**
Trail Making Test A (s)	23.92 (6.42); 19	27.39 (17.04); 18	*p* = .426
Trail Making Test B (s)	57.05 (20.49); 19	82.53 (105.10); 17	*p* = .307
WAIS-III Digit Span Forward	11.26 (2.49); 19	10.22 (1.59); 18	*p* = .138
WAIS-III Digit Span Backward	7.05 (2.32); 19	6.61 (2.00); 18	*p* = .541
Matrix Reasoning – Ordered[1]	10.80 (1.58); 19	10.61 (1.97); 18	*p* = .763
Matrix Reasoning – Random[1]	9.68 (1.73); 19	8.33 (2.95); 18	*p* = .096
VSAT	105.6 (24.00); 19	105.39 (31.69); 18	*p* = .979
Letter Fluency (FAS)[2]	39.89 (8.88); 19	37.44 (10.42); 16	*p* = .456
Category Fluency[2]	43.47 (6.78); 19	43.50 (8.61); 16	*p* = .992
RBANS List Immediate Recall	29.95 (4.74); 19	30.23 (4.83); 13	*p* = .870
RBANS List Delayed Recall	6.89 (2.92); 19	7.31 (2.06); 13	*p* = .664
RBANS Digit Span	**11.79 (2.18); 19**	**10.00 (1.96); 13**	***p* = .024***
RBANS Coding	52. 47 (9.22); 19	47.38 (15.50); 13	*p* = .253

Table 2: Neuropsychological test performances in HC and TBI. [1]Modifications of the Wechsler Adult Intelligence Scale (WAIS) III Matrix Reasoning Test (ordered[increasing] or random difficulty in successive stimulus presentations). [2]From the Delis-Kaplan Executive Functions System (D-KEFS). SD=standard deviation. WAIS=Wechsler Adult Intelligence Scale. RBANS=Repeatable Battery for the Assessment of Neuropsychological Status. VSAT=Visual Search and Attention Test. *Significant at alpha < .05.

A subset of participants in the TBI group (n = 13) was also administered a modification of the n-back task, a widely employed computerized working memory task used to probe goal-direct behaviors, specifically, complex attention and working memory (L. Chang et al., 2001; Kirchner, 1958; Speck et al., 2000). This task involves asking a participant to view a string of letters, and for each, report on whether each

letter was the same as the one viewed immediately prior to the current stimulus (1-back), two before (2-back), or three before (3-back). A 0-back condition, requiring an affirmative response when a particular target stimulus is shown, assesses simple reaction time. To balance sufficient cognitive demand with fatigue/poor effort as well as time limitations, participants received only the 2-back condition. The 2-back administration was manipulated such that "rest" intervals employed in typical paradigms were replaced with prompts asking the participant to answer, by typing onto the computer screen, questions about him/herself. These prompts involved simple autobiographical referencing requiring a combination of simulation (e.g., "Describe your ideal vacation destination") and mentalization (e.g., "Describe how someone would feel if they failed an important exam") abilities, in accordance with recent literature suggesting that these types of self-referential thought engage differential subsystems of the DMN as well as its midline core (Andrews-Hanna et al., 2014). The full list of prompts employed can be found in Appendix A. Responses to these self-referential prompts were not scored, but instead served to keep participants cognitively engaged in internally-focused thought, thereby requiring more effort to switch to goal-directed cognition during 1-back blocks. Therefore, it was intended to be a behavioral analog of the "switching" between the DAN and DMN that is hypothesized to occur in the brain. Outcome measures included both accuracy (percent correct) and reaction time for correct responses.

Image Acquisition and Preprocessing

As part of larger functional and structural neuroimaging study protocols, participants completed two 5-10 minute runs of "rest," in which they were instructed

leave their eyes open and fixate on a crosshair on a projection screen while being scanned; no other visual stimulation was provided. Scan data were acquired using either a Siemens Magnetom Prisma Fit 3.0 T system (Siemens Medical Solutions, Germany) or a Siemens Magnetom Trio 3.0 T system (Siemens, New York, NY). Twelve participants in the TBI group and seven participants in the control group were scanned on the Prisma Fit, while six participants with TBI and 12 controls were scanned on the Trio. Scanner upgrades necessitated the use of two different scanners. Data collection was parameterized to maximize consistency between magnets. Three-dimensional high-resolution T1-weighted magnetization prepared rapid acquisition with gradient echo (MPRAGE) image sequences were optimized across scanners and acquired for each participant to provide high-resolution underlays for functional brain activation. Echo planar imaging (EPI) was used for resting-state functional imaging. EPI sequences were acquired with a 2000 ms repetition time, 30-ms echo time, 90-degree flip angle, 230x230 mm^2 field of view, 80x80 acquisition matrix, and 35 axial slices (4 mm thick) with no gap between slices. Between 150 and 300 functional volumes were collected for each participant. All participants were scanned at the Social, Life, and Engineering Sciences Imaging Center (SLEIC), Pennsylvania State University (University Park, PA). The importance of minimizing head movement during all MRI scanning was communicated to participants prior to scanning and participants were trained in a mock-scanner environment before entering the actual bore.

Preprocessing of structural and resting-state functional data was completed using the Statistical Parametric Mapping 8 (SPM8) software (http://www.fil.ion.ucl.ac.uk/spm/software/spm8/). The first 5 volumes from each participant's time series were

excluded from analyses to accommodate initial signal instability and habituation to the scanner environment. Standard pre-processing steps, including realignment of each individual's functional data to the first functional image of the time series, co-registration of individuals' anatomical and functional images, and a two-step procedure for normalization to Montreal Neurological Institute (MNI) space (parameters derived from T1→MNI for EPI→MNI) was performed. Spatial smoothing with an isotropic Gaussian kernel of 6 mm was applied to images for only seed-voxel connectivity analyses. Given the nature of the planned analytic plan for local PPC connectivity, which included voxelwise analyses, application of a smoothing kernel here would have unduly introduced distortion of signal and lead to inaccuracies in graph metrics. Therefore, spatial smoothing was not performed for PPC graph analyses (note, however, that fMRI data exhibits some "intrinsic" smoothness due to a degree of spatial correlation between voxels even before any smoothing kernel is applied).

Participant movement in the scanner introduces artifacts into fMRI data that pose special challenges for resting-state connectivity analyses (Power, Schlaggar, & Petersen, 2015; Van Dijk, Sabuncu, & Buckner, 2012). While there is no consensus in the field on how to handle motion artifacts, there remains concern that voxelwise regression of the mean fMRI signal, a technique often used to filter out the effects of motion, results in spurious introduction and/or magnification of negative correlations between voxels (Murphy, Birn, Handwerker, Jones, & Bandettini, 2009). Therefore, the current preprocessing pipeline eschewed global signal regression. Instead, in addition to communicating to participants the importance of limiting movement during scanning and inspecting movement in real-time during data collection, the study employed a post-

hoc repair procedure using the ArtRepair toolbox in SPM (Mazaika, Hoeft, Glover, & Reiss, 2009). This program identifies individuals with large, multivolume motion as well as volume-to-volume movements and corrects for perturbations in the BOLD signal due to these conditions. Large movement was addressed by implementing a trigonometric function that applies stronger correction on edge versus central voxels for head translation and rotation. Volume-to-volume motion correction was achieved by interpolating signal from surrounding, unaffected volumes, to create artifact-corrected fMRI volumes following normalization and smoothing (seed-voxel analyses) or only normalization (graph analyses). As recommended by Mazaika et al. (2009), the threshold for acceptable artefactual volumes was set at <25% of each individual's total volume number. Data from 19 of the original 20 eligible HC participants and all TBI participants (n = 18) met motion criteria and were included in the final sample size (see Table 3).

	Scan Motion Correction				
	SD of mean intensity	**Threshold percentage greater than mean intensity[1]**	**# Participants with artefactual volumes/total**	**Median artefactual volumes (range)**	**% Artefactual volumes repaired (sd)[2]**
HC	1.6	1.3	5/19	8 (4-18)	5.6 (4.5)
TBI	1.8	1.3	8/18	7.5 (4-15)	3.3 (2.1)

Table 3. Summary descriptive statistics for head movement in HC and TBI. [1]Denotes average threshold (percentage above mean intensity) automatically set by ArtRepair for additional large motion artifact repair at scan-to-scan threshold of 0.5mm/TR (translational+rotational change between scans). SD=standard deviation. [2]Mean percentage of volumes repaired per individual total volume series.

Motion-corrected volumes were then subject to nuisance signal regression using the aCompCor procedure (Behzadi, Restom, Liau, & Liu, 2007) as implemented in the Conn Toolbox (Whitfield-Gabrieli & Nieto-Castanon, 2012). This method removes

effects of white matter (WM) and cerebrospinal fluid (CSF) signal on the BOLD signal utilizing participant-specific WM and CSF masks, while avoiding the augmentation of negative correlations between voxels associated with global mean signal regression.

PPC Region of Interest Definition

The entire PPC has been mapped cytoarchitectonically (Caspers et al., 2006; Caspers et al., 2008), and this parcellation scheme is publicly available in a probabilistic atlas (SPM Anatomy Toolbox) (Eickhoff et al., 2005). The atlas avails the user of maximum probability maps (MPM), which allow for the definition of non-overlapping subregions that afford better resolution of the PPC than other atlases. In total, 10 contiguous a priori regions of interest (ROIs) in each hemisphere were obtained, and spanned the supramarginal gyrus (PF, PFcm, PFm, PFt, PFop), angular gyrus (PGa, PGp), and the intraparietal sulcus (IPS1, IPS2, IPS3). These ROIs were used in seed-voxel connectivity analyses to examine group differences in PPC→whole brain connectivity. For the subsequent graph theory investigation, the 10 individual PPC ROI masks in each hemisphere were spatially summed and binarized using the Imcalc function in SPM. This resulted in one composite PPC mask per hemisphere, from which a PPC graph adjacency matrix (G_{PPC}) was created. Details on the construction of G_{PPC} are found in the following chapter.

Chapter 5. Data Analyses

Seed-voxel Connectivity of PPC (Aim 1)

Whole-brain connectivity of the PPC subregions described in Chapter IV was performed using the Conn Toolbox (Whitfield-Gabrieli & Nieto-Castanon, 2012). Because conducting independent tests with each PPC subregion— totaling 10 in each hemisphere— would tax statistical thresholds, three mixed-design two-way analysis of variance (ANOVA) models were specified in each hemisphere, corresponding to the three networks of interest. Based on literature reviewed earlier in this document, ROIs were grouped in the following manner and served as levels of the independent factor (ROI) in each model: DMN seeds included PGa and PGp; DAN seeds included IPS1, IPS2, and IPS3; and FCN seeds included PF, PFcm, PFm, PFop, and PFt. Statistical thresholds for omnibus tests were set at a voxel-level (height) threshold of $p<0.005$ and an FDR-corrected cluster (extent) threshold of .05. When appropriate, post-hoc t-tests were employed with an FDR-corrected alpha level of .05, correcting for the number of seeds examined in each analysis, to investigate effects associated with each individual seed.

Graph Theory (Aim 2)

Graph theory offers a powerful approach to studying complex networks and has been applied widely in the biological sciences. The most fundamental elements of a graph are its vertices, or nodes, and edges, the connections between those nodes. In reference to functional brain networks, brain regions assume the position of nodes, while edges are the functional connections between those regions (or the linear

correlation of their time series). Once a brain connectivity graph is constructed, several metrics may be calculated to delineate its network structure. These metrics typically are of three different types: segregation, integration, and influence (Sporns, 2013). Measures of segregation characterize distinct functional units within networks and their relative independence from larger network behavior, In the current study, *modularity*, which falls within the class of segregation metrics, was used to parcellate the PPC into functional subcomponents. Measures of integration quantify the extent to which individual nodes communicate with other nodes in the network at large (e.g., the efficiency of the entire network), and measures of influence denote the relative significance of individual nodes in a network (an indication of hubness), although it should be noted that these metrics are at times both consumed under the category of integration indices (Rubinov & Sporns, 2010). The current study examined strength, global efficiency (integration), and betweenness centrality (influence) to multidimensionally characterize PPC network functionality in controls and TBI.

All graph theory analyses were conducted via in-house scripts, specifically designed for the current analyses and incorporating publicly available packages within the R statistical software (R Core Team, 2013). R packages and functions utilized are referenced in the proceeding sections. For software developed in-house, commented code is available as Supplementary Documents 1 and 2.

Construction of the PPC Graph Adjacency Matrix (G_{PPC})

In keeping with view that PPC functioning reflects the confluence of functional systems, a spatially constrained approach to graph construction was adopted. This

involved the imposition of a three-dimensional lattice framework on the combined PPC ROI, such that only the faces, edges, and corners of each voxel were considered as valid connections, amounting to 26 total possible connections per voxel. Thus, each voxel represented a node in the adjacency matrix. This matrix was thresholded to include only connections, operationalized as absolute-value Pearson correlations between voxel time series, that met the significance criterion of FDR-corrected alpha = 0.05. A lattice constraint ensured that subsequently constructed modules by the modularity algorithm were contiguous, as would be expected in a circumscribed region like the PPC; by contrast, disjointed modules are more appropriate in whole-brain graphs, where the goal is instead to identify distributed (spatially separated) networks.

While a lattice network was used for both modularity and subsequent investigation of G_{PPC} strength, centrality, and global efficiency, preparation of the PPC ROI differed between the two analyses. Because the goal of modularity was to identify consistent modules across individuals for potential analyses on group-averaged data, the PPC ROI implemented here was uniform across all individuals (i.e., not masked by participant-specific grey matter). This was done to minimize the effects of individual differences in cortical anatomy, as construed by segmentation algorithms, on modular organization and to facilitate interindividual comparisons of this organization. By contrast, examination of PPC strength, centrality, and efficiency is not spatially dependent. Thus, participant-specific grey matter masks were employed to constrain the PPC ROI for these later analyses, which generated conservative, more precise estimates of graph metrics within each individual that could then be submitted to statistical tests at the group level.

Modularity

A graph can be partitioned into modules of node sets based on the relationships between nodes and their connectivity with the rest of the graph. Essentially, modules refer to groups of nodes that are densely connected to each other, but sparsely connected with the rest of the graph (Newman, 2006). Hence, every module is a "community" of nodes, and the modularity measure of the graph describes the extent to which the graph can be characterized by modular organization. Modularity Q of a graph is given by the equation: $Q = (1/2E)\sum_{ij}(A_{ij}-(k_ik_j/2m))\delta(C_i,C_j)$, where E is the number of edges in the graph, k_i is the degree of node i (see discussion of degree below) and $\delta(C_i,C_j)$ is known as the Kronecker delta function, a dichotomous function that yields a value of 1 if node i is in module C_i and node j is in module C_j, and 0 if these conditions are not met (Rajtmajer, Roy, Albert, Molenaar, & Hillary, 2015). In the brain, identification of modular structure (whether at the whole-brain or regional level) can reveal distinct multi-node units that have different functional specificity (Wang, Zuo, & He, 2010).

The current study employed the Louvain modularity algorithm (Blondel, Guillaume, Lambiotte, & Lefebvre, 2008). The Louvain approach refers to an optimization method that maximizes the modularity value Q in two iterative steps. The first step assigns individual nodes to their own communities and endeavors to optimize local modularity in a "greedy" manner by repeatedly moving a given node i into the community of node j; if no modularity increase is achieved, node i remains in its original community. The second step reapplies the first step on a new network, in which communities from the first step now serve as nodes. The algorithm proceeds until

community reassignments fail to produce any further increase in modularity. In the current study, the function *cluster_louvain* in the igraph package for R was implemented to perform Louvain modularity on G_{PPC} at the individual level.

After implementation of Louvain modularity, spatial similarity of the resulting individual modular structures was compared across participants in each group. This was achieved with an additional custom script, which produced two well-known similarity measures: the Jaccard coefficient (Jaccard, 1912) and the Sorensen coefficient (Sorensen, 1948). Both these metrics quantify data similarity between pairs of individuals, from which an average similarity metric can be obtained for the entire group. The Jaccard coefficient is given by intersection over union, $A \cap B / A \cup B$, where A is the set of voxels in a given module of a participant and B is an analogous set in another participant. Essentially, this provides a ratio of the shared space to the total space in a two-circle Venn diagram. By comparing each module in Participant A with that in Participant B, a single Jaccard coefficient for the pair of individuals is obtained. The Sorensen coefficient is closely related to the Jaccard measure, but gives greater weight to shared voxels in a given module comparison than voxels only present in one individual's module. The Sorensen coefficient is thus quantified as $2(A \cap B) / ((2A \cap B)+A_1+B_1)$, where A_1 and B_1 are the non-overlapping portions of Participant A and Participant B's voxel set, respectively. Jaccard and Sorensen coefficients were used to gauge appropriateness of averaging across individuals' time series data and conducting further graph theoretical analyses on the resulting group-level correlation maps.

Degree of G_{PPC}

The degree of a node is the sum of the number of edges incident on that node. In other words, it is the number of connections of a given node. Degree is therefore a fundamental measure of hubness, and is given by $deg_i = \mathrm{N}(i)$, where N is the neighborhood of the number of edges incident to node *i*. Summing the value of deg_i across all nodes and dividing by the number of nodes gives the average degree of the network, which, along with the number of nodes, is also an index of network size. Network size influences other graph theoretical metrics, and thus may confound tests of group differences. In the current study, the function *degree* in the igraph package for R was implemented to compute the degree of each node in each individual's G_{PPC}, and was used to assess differences in network size between the HC and TBI groups.

Strength of G_{PPC}

Nodal strength is equated with the weighted nodal degree of a network (i.e., the sum of the weights incident on each node averaged across nodes). When this measure is divided by the number of edges in a network, it represents the average between-node connection strength in the entire network. Network strength of a weighted graph *G* is therefore the sum of all suprathreshold edge weights in the graph divided by its number of edges. It is given by $S_G = w\mathrm{N}(i)/E$, which is identical to the formula presented above for degree, but now incorporates the weights *w* of all incident edges and a divisor of the total number edges *E*. This metric was used to identify hyper- or hypo-connectivity within G_{PPC} between hemispheres, as well as in TBI versus controls.

Global Efficiency of G_{PPC}

The shortest path length between two nodes is a popular graph metric that characterizes how closely affiliated the two nodes are, and in the context of functional brain networks, refers to how many connections are traversed to reach region B from a given region A. The average of the shortest path lengths between all possible node pairs thus provides a measure of node-to-node integration within the network. Directly related to the average shortest path length is global efficiency, which is simply its inverse (Latora & Marchiori, 2001). Global efficiency E_{glob} is given by $E_{glob}(G) = 1/N(N-1)\Sigma_{i\neq j\in G}(1/d_{ij})$, where d_{ij} is the shortest path length between nodes *i* and *j* in a graph *G* with *N* nodes and *E* edges. In the current study, the function *graph.efficiency* in the brainGraph package for R was implemented to compute the global efficiency of G_{PPC} in each individual. Global efficiency was used to characterize the extent of nodal integration within G_{PPC}. Both hemispheric and group effects were examined.

Weighted Betweenness Centrality of G_{PPC}

Hubness is sometimes operationalized as betweenness centrality, or the number of times a node is traversed in the shortest route from one node to another in the graph. In a weighted network, shortest routes refer to those connection paths that minimize the total (summed) connection strength of each edge traveled. Here, weights of the connections are treated as costs, with the goal being to minimize the utilization of costly connections in determining shortest path. Thus, “cost” here does not convey information about metabolism or distance, but is a general term in network science referring to how expensive— in correlation weights— a connection is. Weighted betweenness centrality of a node a measure of how frequently the node stands between two other nodes in a

minimally costly path. This metric can be averaged over all nodes to arrive at the overall "centrality" of the graph. Weighted betweenness centrality B^w of a node *i* is expressed as $B^w_i = \Sigma_{m \neq i \neq n \in G} (\sigma^w_{mn}(i)/\sigma^w_{mn})$, where $\sigma^w_{mn}(i)$ is the number of weighted shortest paths from node m to node n passing through node *i*, and σ^w_{mn} is the total number of weighted shortest paths from node m to node n; i.e., the ratio of shortest paths traversing node *i* to total shortest paths. Because betweenness centrality scales with the number of node pairs under consideration, a normalized version that standardizes the calculation based on node pairs (excluding the node of interest) can be used to facilitate comparisons of this metric between networks. This is given by $\text{norm}B^w_i = (2B^w_i)/(N*N-3*N+2)$, where *N* is the total number of nodes in the graph. In the current study, for each individual, the function *betweenness* in the igraph package for R was implemented to compute the normalized weighted betweenness centrality of each G_{PPC} node, which was then averaged to obtain the centrality of G_{PPC}. Weighted betweenness centrality was used to assess the extent to which each individual G_{PPC} node, on average, influences interactions between other, spatially distributed nodes.

Statistical Analyses of Graph Metrics and Behavior (Aims 2 and 3)

Hemispheric and group differences in G_{PPC} modularity were examined using two-way repeated measures analysis of variance (ANOVA), with group as a between-subjects factor and hemisphere as a within-subjects factor. Group differences in level of interindividual variability as measured by Jaccard and Sorensen coefficients were probed with independent samples t-tests.

Hemispheric and group differences in G_{PPC} strength, centrality, and global efficiency were examined using two-way repeated measures multivariate ANOVA (MANOVA), with group as a between-subjects factor, hemisphere as within-subjects factor, and centrality, strength, and global efficiency as multivariate outcomes. Post-hoc univariate tests were conducted with Bonferroni correction for multiple comparisons. Correlations between neuropsychological, modified 2-back, and graph theoretical metrics were obtained using Pearson (*r*) coefficients. Multiple linear regression models were constructed for behavioral and graph theoretical measures found to have the strongest relationships in correlation analyses. All statistical analyses of graph theory metrics were performed in IBM SPSS Statistics Version 22.0 (IBM Corp., 2013).

Statistical Thresholding (all analyses)		
Analysis	***p*-threshold**	**Correction**
Seed-voxel	.005 (voxel)	.05 cluster-FDR; post-hoc comparisons corrected for # seeds at .05 FDR
Overlap coefficients	.05	Bonferroni
G_{PPC} MANOVA	.05	post-hoc Bonferroni
G_{PPC} strength & neuropsychological test performance	.05	Bonferroni; non-surviving larger effect sizes considered for interpretation
All G_{PPC} metrics and 2-back reaction time	.05	Bonferroni; non-surviving larger effect sizes considered for interpretation

Table 4: Statistical thresholds and corrections used for primary and post-hoc analyses. FDR=false discovery rate.

Chapter 6. Results

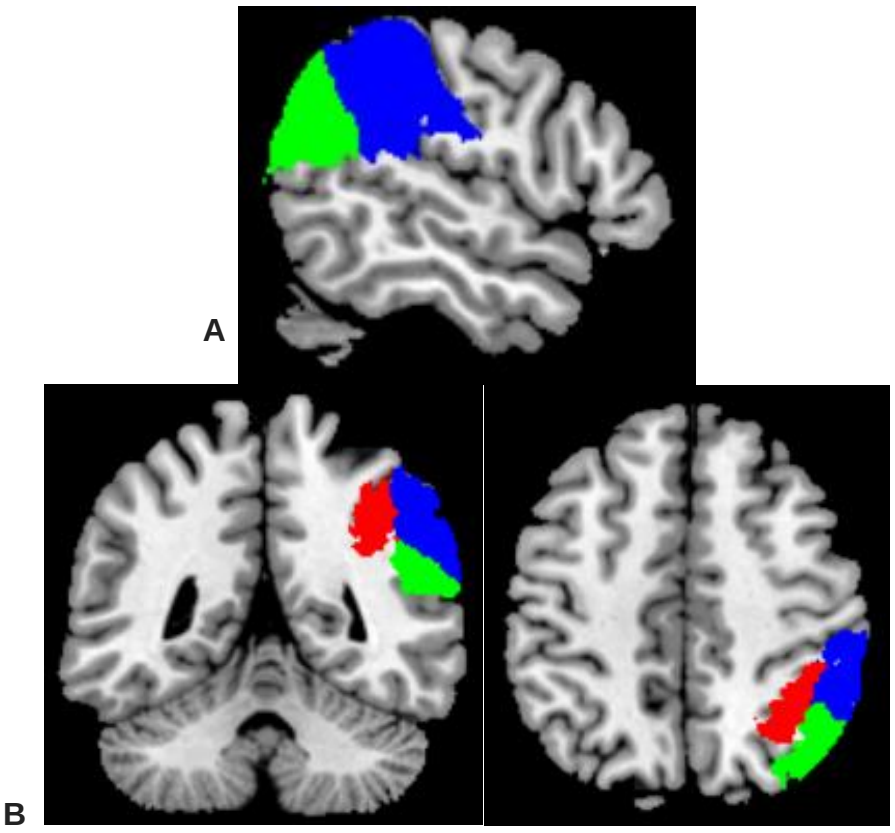

Figure 1. The PPC defined in this study (right hemisphere shown in all views). MNI coordinate view in: A. (sagittal) 146,76,105; B. (coronal) & C. (axial) 84,78,119. Images illustrate the PPC with colored subdivisions (anterior, posterior, superior) according to their whole-brain network affiliations (green=DMN-aligned, red=DAN-aligned, blue=FCN-aligned). Subregions within these subdivisions were used in seed-voxel analyses. The PPC graph for network analyses reflected a summation of all constituent PPC regions.

Examining Aim 1, Hypotheses 1 and 2: Group Differences in Whole-brain Connectivity of PPC Subregions

In the left PPC (see Table 5), and in TBI relative to controls, DMN-aligned subregions showed increased positive connectivity with frontal DMN regions, including anterior cingulate and medial prefrontal cortices. Post-hoc analyses revealed significant effects for both DMN subregions (PGa and PGp). Similarly, FCN-aligned subregions showed robust connectivity increases with remote regions of the FCN, including the

right frontal pole and right insula, in TBI. Specifically, FCN-aligned subregions centrally located within the PPC (PF, Pfm) were significant for the frontal pole finding, while all but PFm were significant for the insula effect.

While no group differences were found for positive connectivity of DAN-aligned subregions, IPS1 and IPS3 showed increased negative connectivity to areas outside the DAN in TBI compared to controls. Specifically, a region encompassing portions of the cuneus and precuneus of the FCN was identified. There was also decreased negative connectivity in TBI versus controls between IPS1/IPS2 and sensorimotor areas (paracentral lobule).

Group Differences in Left PPC Seed-voxel Connectivity						
Left PPC seed subset	**ANOVA F**	**[Cluster peak coordinates][1], name (#voxels)**	**Seed**	**Post-hoc t**	**P-value[2] ; beta**	**Directionality**
DMN-aligned	df=(2, 70) 5.72	[14, 40, 34] L ACC/mPFC (138)	*PGa*	5.73	<.001 ; .23	TBI > HC**
			PGp	3.79	<.001 ; .16	TBI > HC**
		[16, 49, 13] R ACC/mPFC (86)	*PGa*	5.92	<.001 ; .22	TBI > HC**
			PGp	2.84	.006 ; .11	TBI > HC*
DAN-aligned[3]	df=(3, 105) 4.53	[10, -62, 28] B PreCu/Cu (166)	*IPS1*	2.45	.016 ; .11	TBI > HC*
			IPS2	-1.40	0.164 ; -.06	HC > TBI
			IPS3	2.46	0.031 ; .11	TBI > HC*
		[7, -41, 67] B PCL (116)	*IPS1*	-3.33	.002 ; -.13	HC > TBI*
			IPS2	-4.15	<.001 ; -.16	HC > TBI**
			IPS3	-.87	.388 ; -.03	HC > TBI
FCN-	df=(5, 175)	[19, 55, 31]	*PF*	2.05	.042 ; .08	TBI > HC*

aligned	3.48	R Frontal Pole (164)	*PFcm*	.17	.868 ; .01	TBI > HC
			PFm	6.30	<.001 ; .24	TBI > HC**
			PFop	-.73	.468 ; -.03	HC > TBI
			PFt	-1.27	.207 ; -.04	HC > TBI
		[37, 1, 2] R Insula (83)	*PF*	2.69	.016 ; .10	TBI > HC*
			PFcm	4.45	<.001 ; .15	TBI > HC**
			PFm	1.41	.161 ; .05	TBI > HC
			PFt	4.24	<.001 ; .14	TBI > HC**
			PFop	4.72	<.001 ; .15	TBI > HC**

Table 5: Seed-voxel results from left PPC subregions. [1]Coordinates in Montreal Neurologic Institute (MNI) space. [2]FDR-corrected p-value. [3]Results from this seed reflect differences in *negative* connectivity. L=left, R=right. ACC=anterior cingulate, mPFC=medial prefrontal cortex, PreCu=precuneus, Cu=cuneus, PCL=paracentral lobule. **Significant at alpha < .001. *Significant at alpha < .05.

There were no significant group differences involving the DMN- and DAN-aligned subregions in the right PPC (see Table 6). However, increased connectivity in TBI was observed between FCN-aligned subregions and the right orbitofrontal cortex, another FCN member region. Effects were significant for all but the PFcm subregion.

Group Differences in Right PPC Seed-voxel Connectivity						
Right PPC seed subset	**ANOVA F**	**[Cluster peak coordinates][1], name (#voxels)**	**Seed**	**Post-hoc t**	**P-value[2] ; beta**	**Directionality**
DMN-aligned	No significant group differences					
DAN-aligned	No significant group differences					
FCN-aligned	df=(5, 175) 3.48	[46, 19, -17] R OFC (103)	*PF*	5.24	<.001 ; .22	TBI > HC**
			PFcm	1.69	.093 ; .07	TBI > HC
			PFm	4.85	<.001 ; .20	TBI > HC**
			PFop	2.60	.010 ; .10	TBI > HC*
			PFt	3.11	.002 ; .12	TBI > HC**

Table 6: Seed-voxel results from right PPC subregions. [1]Coordinates in Montreal Neurologic Institute (MNI) space. [2]FDR-corrected p-value. **Significant at alpha < .001. *Significant at alpha < .05.

Examining Aim 2, Hypothesis 1: Modularity of G_{PPC} Within and Between Groups

Across the full sample, age was not related to modularity. Additionally, size of G_{PPC}— operationalized as the number of nodes in each individual's G_{PPC}— was not related to modularity *Q* in the left hemisphere across groups ($r = 0.09$, $p = 0.61$). However, a moderate correlation was observed between modularity and right G_{PPC} size *(*$r = 0.35$, $p = 0.03$). Consequently, left and right hemisphere modularity scores were multiplied by their respective G_{PPC} sizes before being entered into a mixed-design ANOVA to examine group and hemispheric differences in modularity. Results did not reveal a significant hemisphere by group interaction. However, a significant main effect of hemisphere was observed ($F_{1,35} = 168.37$, $p < 0.001$, partial $\eta^2 = 0.83$). Comparison of marginal means revealed greater right than left G_{PPC} modularity across the HC and TBI groups (means = 1067.12 [right] and 959.56 [left]). There was no main effect of group on the scaled modularity scores. ANOVA results are given in Table 7. Within the TBI group, time-post injury showed moderate negative correlation with modularity for only the left hemisphere ($\rho = -0.611$, $p = 0.007$).

G_{PPC} Modularity – ANOVA, Hemisphere by Group				
	L modularity mean[1] (SD)		**R modularity mean[1] (SD)**	
HC	952.415 (73.392)		1062.441 (103.053)	
TBI	966.700 (41.000)		1071.806 (45.692)	
	ANOVA $F_{1,35}$	**P-value**	**Partial η^2**	**Directionality**

Hemisphere	168.365	<.001	.828	R > L**
Group	.294	.591	.008	TBI > HC
Hemisphere x Group	.088	.768	.003	--

Table 7: Modularity results by hemisphere and group. [1]Adjusted score, scaled by number of vertices. L=left, R=right. SD=standard deviation. **Significant at alpha < .001.

Across both hemispheres within the HC and TBI groups, Jaccard and Sorensen values suggested modest interindividual consistency (see Table 8), although this observation was not based on any stringent cutoff. Independent samples t-tests revealed significant between-group differences in both overlap coefficients across hemispheres, indicating that there was more variability in modular structure in the HC group compared to the TBI group (Table 8; Figure 2).

G_{PPC} Interindividual Variability – Overlap Coefficients			
	HC mean (SD)	**TBI mean (SD)**	**Group comparison**
Left Jaccard	.4903 (.05621)	.5193(.05816)	t_{322} = -4.549, p < .001**†
Left Sorensen	.6339 (.05246)	.6618 (.05123)	t_{322} = -4.834, p < .001**†
Right Jaccard	.4384 (.05879)	.4710 (.06013)	t_{322} = -4.925, p < .001**†
Right Sorensen	.5877 (.05456)	.6187 (.05423)	t_{322} = -5.127, p < .001**†

Table 8: Modularity overlap scores within groups and group differences. SD=standard deviation. **Significant at alpha < .001. †Passed Bonferroni correction.

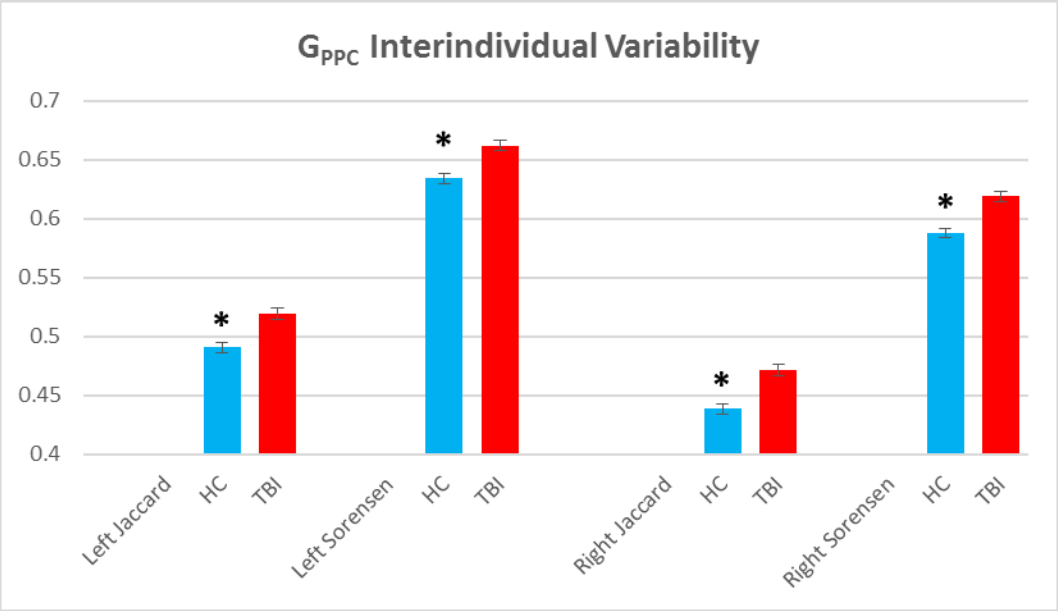

Figure 2: Jaccard and Sorensen coefficients by group and hemisphere. Note that higher scores represent less within-group variability. Error bars reflect standard error. *Group difference significant at alpha < .001 and passed Bonferroni correction.

Examining Aim 2, Hypothesis 2: G_{PPC} Strength, Centrality, and Global Efficiency Within and Between Groups

Average degree of G_{PPC} did not differ between HC and TBI groups for either hemisphere (L: t_{35} = -0.21 p = 0.84; R: t_{35} = -1.11, p = 0.27). There were also no significant differences in number of nodes in grey matter-masked G_{PPC} between groups (L: t_{35} = -0.03 p = 0.98; R: t_{35} = -0.74, p = 0.46). Across all participants, age was not correlated with any of the graph metrics of interest (strength, centrality, efficiency) in either hemisphere. In the TBI group, time post-injury also did not show any associations with these graph metrics.

MANOVA revealed a significant main effect of hemisphere on the three G_{PPC} metrics treated as multivariate effects: strength, centrality, efficiency, with a large effect

size (Wilks' lambda $F_{3,33} = 12.05$, $p < 0.001$, partial $\eta^2 = 0.52$; see Tables 9 and 10). This effect was not significant for the independent variable of group. A hemisphere by group interaction did not reach significance (Wilks' lambda $F_{3,33} = 1.82$, $p = 0.16$, partial $\eta^2 = 0.14$). In post-hoc univariate analyses, there was a significant main effect of hemisphere on centrality (left > right, $F_{1,35} = 35.84$, $p < 0.001$, partial $\eta^2 = 0.51$) as well as strength (right > left, $F_{1,35} = 11.30$, $p = 0.002$, partial $\eta^2 = 0.24$). However, the latter finding was observed in the context of a significant group by hemisphere interaction for strength, such that the TBI group showed disproportionately large connection strength of the right versus left G_{PPC} compared to healthy controls ($F_{1,35} = 5.67$, $p = 0.02$, partial $\eta^2 = 0.14$) (Figure 3).

G_{PPC} Summary Statistics			
		HC mean (SD)	**TBI mean (SD)**
Strength	*Left*	.499168 (.045052)	.522136 (.054981)
	Right	.504009 (.044448)	.550513 (.059817)
Centrality	*Left*	.010735 (.001445)	.010590 (.000941)
	Right	.009694 (.001252)	.009395 (.000809)
Global efficiency	*Left*	.167335 (.004139)	.167472 (.002439)
	Right	.167473 (.003810)	.168625 (.002993)

Table 9: Descriptive statistics for PPC graph metrics in HC and TBI. SD=standard deviation.

G_{PPC} MANOVA, Hemisphere by Group						
	Omnibus statistics	**G_{PPC} measure**	**Univariate $F_{1,35}$**	**P-value**	**Partial η^2**	**Directionality**
Hemisphere	$F_{3,33} = 14.705$	*Strength*	11.302	.002	.244	R > L*†
	$p < .001$**	*Centrality*	35.834	<.001	.506	L > R**†

	partial η^2 = .572	*Global efficiency*	1.341	.255	.037	R > L
Group	$F_{3,33}$ = 1.678	*Strength*	4.633	.038	.117	TBI > HC*
	p = .191	*Centrality*	.460	.502	.013	HC > TBI
	partial η^2 = .132	*Global efficiency*	.432	.515	.012	TBI > HC
Hemisphere x Group	$F_{3,33}$ = 1.815	*Strength*	5.674	.023	.140	TBI: R > L*
	p = .164	*Centrality*	.170	.682	.005	--
	partial η^2 = .142	*Global efficiency*	.829	.369	.023	--

Table 10: Within and between group differences in PPC graph metrics. L=left, R=right. **Significant at alpha < .001. *Significant at alpha < .05. †Passed Bonferroni correction.

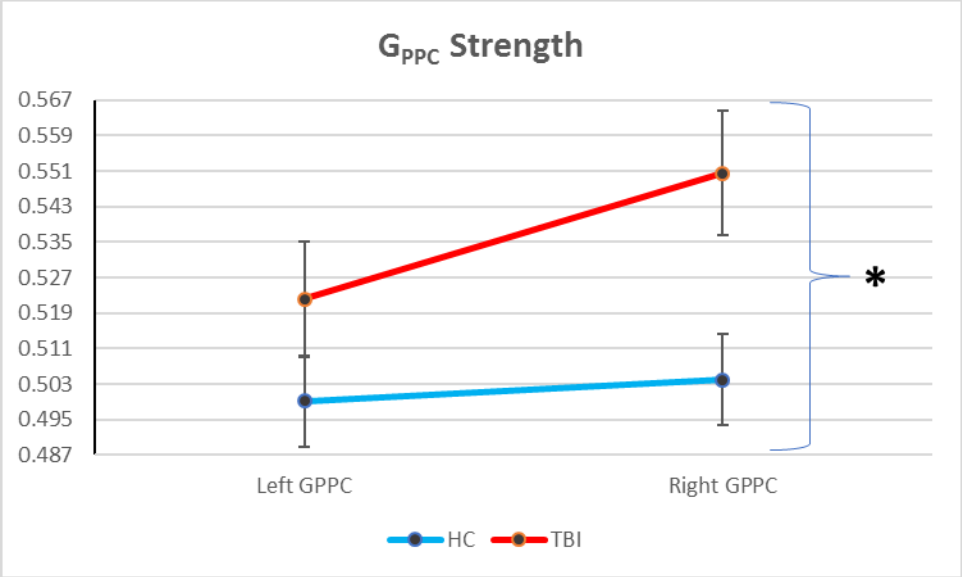

Figure 3: Left and right G_{PPC} strength in HC and TBI groups. Error bars reflect standard error. *Interaction significant at alpha < .05, uncorrected, with moderate effect size (partial η^2 = 0.14).

Examining Aim 3, Hypothesis 1: G_{PPC} Strength and Neuropsychological Functioning

Based on observed group differences in right G_{PPC} strength, this metric was targeted for behavioral analyses with neuropsychological test scores. In the full sample, correlational analyses revealed a significant inverse relationship between right G_{PPC}

strength and performance on the RBANS Digit Span subtest (r = -0.43, p = 0.02). Recall from earlier that this was the only test performance that differed between groups, with the TBI group showing significantly worse performance. Follow-up analyses within groups revealed that the correlation between network strength and RBANS Digit Span was being driven solely by the TBI group (Table 11); that is, strength was not related to RBANS Digit Span in controls. Although falling short of passing statistical correction, the magnitude and significance of this finding was fairly robust (r = -0.70, p = 0.008; Figure 4).

Right G_{PPC} Strength and Neuropsychological Test Performance in TBI		
Test	**Pearson *r*; n**	**p-value**
Trail Making A (s)	.324; 18	p = .190
Trail Making B (s)	.266; 17	p = 303
WAIS-III Digit Span Forward	-.105; 18	p = .679
WAIS-III Digit Span Backward	-.054; 18	p = .832
Matrix Reasoning - Ordered	-.019; 18	p = .941
Matrix Reasoning - Random	.287; 18	p = .248
VSAT	-.264; 18	p = .289
Letter Fluency (FAS)	-.338; 16	p = .201
Category Fluency	-.186; 16	p = .491
RBANS List Immediate Recall	-.009; 13	p = .977
RBANS List Delayed Recall	.015; 13	p = .961
RBANS Digit Span	**-.697; 13**	***p* = .008***
RBANS Coding	-.064; 13	p = .835

Table 11: Correlations between right G_{PPC} strength and performance on neuropsychological tests. *Significant at alpha < .05, uncorrected.

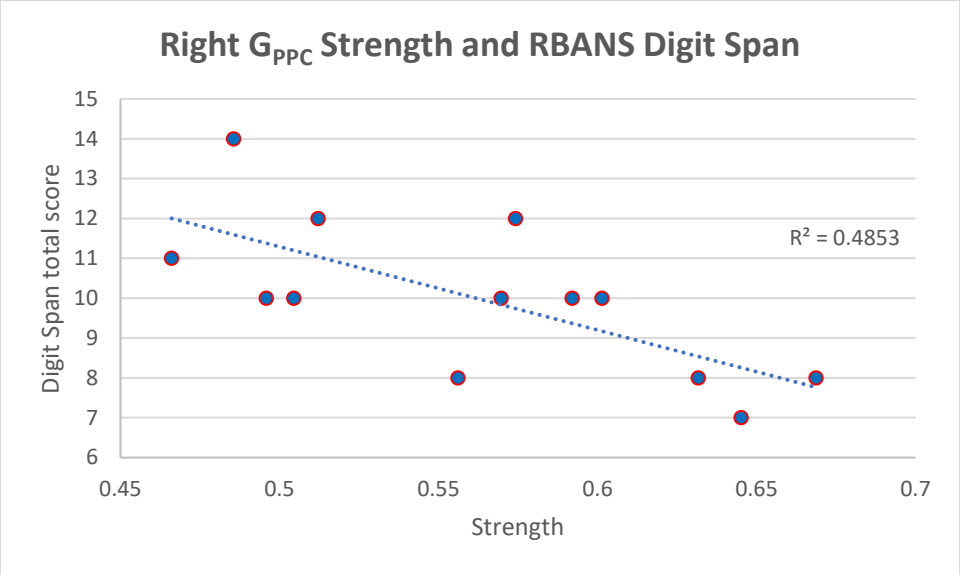

Figure 4: Relationship between G_{PPC} strength and RBANS Digit Span performance.

Examining Aim 3, Hypothesis 2: G_{PPC} Metrics and N-back Performance

Of the three G_{PPC} graph metrics from each hemisphere, global efficiency of the right G_{PPC} showed a strong relationship with 2-back reaction time, such that greater efficiency was strongly associated with faster reaction time ($r = 0.72$, $p = 0.008$; Figure 5). This effect passed Bonferroni correction for all comparisons with reaction time (Table 12). An additional significant positive association was noted between 2-back reaction time and normalized betweenness centrality of right G_{PPC}, although this relationship did not pass statistical correction. A highly left-skewed distribution of 2-back hit rate combined with the relatively small sample size limited the variance available to examine associations between 2-back accuracy and graph metrics.

Graph Metrics and 2-back Reaction Time in TBI (n=12)		
G_{PPC} Metric	**Pearson *r***	**p-value**
Left strength	.196	p = .541
Right strength	.301	p = .341
Left efficiency	-.085	p = .792
Right efficiency	**-.724**	***p* = .008*†**
Left betweenness centrality[1]	.180	p = .576
Right betweenness centrality[1]	**.576**	***p* = .050***

Table 12: Correlations between right G_{PPC} global efficiency and 2-back reaction time. [1]Normalized, weighted measure. *Significant at alpha < .05. †Passed Bonferroni correction.

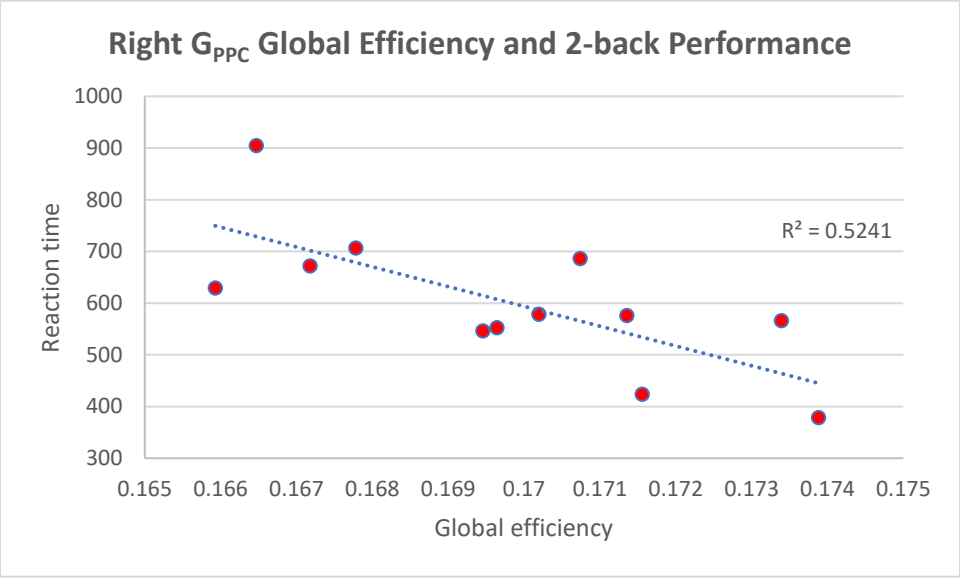

Figure 5: Relationship between G_{PPC} global efficiency and 2-back performance.

Chapter 7. Discussion

The functional heterogeneity of the PPC, characterized by a confluence of subregions participating in different networks, makes it a prime candidate for information consolidation and transfer between networks. Indeed, this notion is supported by the identification of the PPC as a “hub” in previous literature examining whole-brain connectivity (Buckner et al., 2009; Cole, Pathak, & Schneider, 2010; Sato et al., 2016; Tomasi & Volkow, 2010, 2011). By probing the functional architecture of this local PPC network, the dissertation endeavored to clarify the role of smaller scale connectivity patterns in healthy individuals and within the context of global network perturbance as seen in traumatic brain injury. Although rarely implicated as a site of direct structural damage, the PPC’s heteromodal nature was thought to be relevant to the diverse clinical sequelae of TBI, and thus, a potential instance of functional alteration in response to structural disruption in remote areas (Bonnelle et al., 2012; Jilka et al., 2014). Principal questions of interest were whether local functional properties of the PPC reveal information distinct from that obtained with more typical whole-brain analyses, how they relate to cognitive functioning, and what they may indicate about network alteration and recovery after neurologic trauma.

Results of the current work represent three major findings. First, traditional seed-voxel connectivity analyses revealed strong evidence of hyperconnectivity between PPC subregions and remote brain areas in TBI relative to controls, although these effects were most robust in the left-lateralized PPC. Secondly, graph theoretical analyses showed greater within-PPC strength and reduced centrality in the right hemisphere relative to the left across the full sample, with a disproportionately greater

hemispheric split in strength for the TBI group compared to controls. These effects were observed in the context of generally preserved PPC modular structure, but increased interindividual spatial consistency of modular structure in TBI than controls. Finally, PPC strength and efficiency was related to measures of cognitive functioning in TBI, highlighting the relevance of local network dynamics to behavior in neurologic disruption. These findings are further explicated and synthesized in the following sections.

Whole-brain Connectivity of PPC Subregions

In left-lateralized PCC, hyper--positive connectivity was seen in TBI, relative to controls, between DMN-aligned subregions and remote DMN member regions, including the ventral anterior cingulate and medial prefrontal cortices. FCN-aligned PCC subregions showed increased connectivity with the frontal pole and insula (left PPC) and orbitofrontal cortex (right PPC), regions commonly implicated in the putative FCN. These results are consistent with a growing body of TBI literature demonstrating chronic hyperconnectivity patterns, particularly within major functional networks such as the DMN and FPN, at rest (Hillary, Rajtmajer, et al., 2014; Hillary et al., 2015; Palacios et al., 2013; Sharp et al., 2011; Shumskaya, van Gerven, Norris, Vos, & Kessels, 2017; Tang et al., 2012; Venkatesan et al., 2015; see also Caeyenberghs, Verhelst, Clemente, & Wilson, 2016). Increased functional synchronization has been such a robust finding in not only TBI, but other neurologic disorders, that it is has been posited as a direct consequence of neurologic disruption (Hillary et al., 2015; Hillary & Grafman, 2017).

On the other hand, it has also been observed that there is increased negative connectivity between regions of different networks (Bernier et al., in press; Venkatesan et al., 2015), or impaired functional integration on the whole-brain level in TBI (Caeyenberghs et al., 2016; Han, Chapman, & Krawczyk, 2016). Consistent with this idea, the current study found increased negative connectivity between DAN-aligned subregions in the left PPC and a key component of the FCN, the precuneus. Related observations were made recently by Sours and colleagues (2017) in one of the only investigations of lateral parietal lobe functional connectivity in moderate-severe TBI to date. These authors noted reduced connectivity between the intraparietal sulcus and other DAN regions as well as select regions of the FCN, which they interpreted as deficient multisensory processing and integration. Thus, the current findings provide some corroborating evidence for decreased cross-network communication in TBI *at the whole-brain level*.

Taken together, seed-voxel results support a mechanical-type shift in network dynamics after TBI, such that greater within-network "push" is accompanied by between-network "pull." We have previously proposed that such a skew may reflect harnessing of the brain's natural functional architecture to facilitate recovery (Hillary et al., 2011; Venkatesan et al., 2015), although the way in which this might be accomplished has remained unclear. Using whole-brain graph theoretical approaches, former studies in healthy individuals have observed that the brain is organized into relatively distinct functional modules (Bullmore & Sporns, 2009; Cao et al., 2014; Sporns, 2011), mapping onto components of known functional networks (Bertolero, Yeo, & D'Esposito, 2015; He et al., 2009; Meunier, Lambiotte, Fornito, Ersche, &

Bullmore, 2009). This setup appears to support cognitive functioning in both neurologically intact (Alavash, Doebler, Holling, Thiel, & Giessing, 2015; Dwyer et al., 2014) and impaired (T. Y. Chang et al., 2016; Duncan & Small, 2016) individuals. However, cognitive efficiency, particularly in higher-order functions such as cognitive flexibility and reasoning, is also dependent on robust cross-network communication. For example, Yue et al. (2017) recently demonstrated that stronger whole-brain modularity was related to better performance on relatively simple tasks, that is, those that placed minimal demands on executive functioning. However, this relationship was inverted for complex, executively-taxing tasks, where greater modularity predicted worse performance. Thus, it would appear that a negotiation of within and between network communication is required to support diverse cognitive functions. The question at this juncture, and one that the dissertation aimed to address with graph theoretical analyses, is whether the loss of the cross-network communication at the whole-brain level in TBI can also be identified at local points of network convergence. If so, this would suggest that local network fragmentation underlies and potentially predicts global network dysfunction in TBI.

Modularity of the Local PPC Network

Mirroring modular functional organization at the whole brain level, the current study results revealed high modularity of the PPC in both the control and TBI groups, with relatively greater right hemispheric modularity than left across groups. There were no group differences in the level of modularity between groups, nor were there any differences in average nodal degree of the PPC network in later analyses, a finding which resonates with previous literature describing relatively preserved connection

number vis-à-vis changes in connection strength (Nakamura et al., 2009). Although the present modularity analysis did not offer any greater granularity in identifying functional PPC subdivisions than is afforded by a priori ROI definitions (i.e., on average, only about 10 modules were identified in either group), these figures are consistent with previous attempts at parcellating portions of the posterior parietal cortex (Igelstrom & Graziano, 2017; Zhang & Li, 2014).

Unanticipated findings were obtained from analyses examining interindividual variability. In using Jaccard and Sorensen coefficients to examine interindividual concordance in (spatial) modular structure, it is important to note that there is no gold standard for determining “acceptable” overlap. Furthermore, because the number of modules retrieved across individuals was not sufficiently high enough to explore modules as nodes in group-averaged time series, the primary goal in overlap analyses became the investigation of between-group differences in modular consistency within groups. Essentially, this is a question of how the level of interindividual variability in modular structure within a group differs between groups. Contrary to the intuitive notion that the inherently heterogeneous nature of TBI across individuals would engender greater interindividual variability, results revealed significantly more consistency in the modular organization of PPC among members of the TBI group than those of the control group. The extent to which greater interindividual similarity reflects greater concordance with anatomic boundaries of the PPC subregions in the TBI group remains unclear, and presents an intriguing avenue for future investigation.

Strength, Centrality, and Efficiency within the Local PPC Network

When considered as a cohesive network, the selected graph metrics of the PPC network showed significant within and between group effects with fairly remarkable effect sizes. These were particularly notable considering that the magnitude of these effects in terms of raw values was quite subtle.

Although no lateralization hypotheses were made at the outset of the study, it was nonetheless important to examine hemispheric differences given evidence for lateralization of some brain networks. Specifically, this includes a right-lateralized system known as the ventral attention network, which shares significant conceptual and spatial overlap with the FCN (see Corbetta & Shulman, 2002; Fox et al., 2006; Vossel et al., 2014). In the current study, there was greater strength but reduced weighted betweenness centrality of the right PPC relative to the left. This suggests not only more robust connections in the right PPC, but also a diminished tendency towards hubness, highlighting the relatively reduced importance of individual nodes in maintaining local network integrity. Because lateralization of these PPC properties appears to be an inherent part of functional brain organization (i.e., to some extent independent of neurologic status), the current findings suggest a special role of the right PPC in heteromodal integration. Such an interpretation is informed by seed-voxel findings above, where hyperconnectivity in TBI was consistently noted across hemispheres within the FCN, and from both FCN subregions only to right frontal areas of the rest of the FCN. In the context of evidence for lateralization of the FCN and its role in integrating information from divergent networks (DMN, DAN), it is possible that greater strength and lower centrality of the right PPC reflects a microcosmic instance of information transfer mediated by local FCN constituents in the PPC. This perspective is

reminiscent of a well-established literature base describing neural recruitment of right hemispheric regions in the face of increased cognitive challenge in healthy aging populations (Cabeza et al., 1997; Cappell, Gmeindl, & Reuter-Lorenz, 2010; Grady, McIntosh, & Craik, 2005; Reuter-Lorenz et al., 2000), and also in TBI (see Hillary, Genova, Chiaravalloti, Rypma, & DeLuca, 2006, for a review).

Although the connection strength of the right PPC was increased compared to the left PPC across groups, this increase was disproportionately greater in TBI. It is noted that local hyperconnectivity, while less frequently explored, is not a new concept in TBI (Harris et al., 2016; Venkatesan et al., 2015). However, this finding was contrary to the expectation that the integrative function of the PPC would be degraded in TBI and thus show overall decreased local network connectivity. Moreover, recent evidence suggests that hyperconnectivity in TBI is not due to a generalization, or dedifferentiation, of connectivity patterns (Bernier et al., in press).

The effects of widespread neural disruption are complex and may not follow a consistent pattern or have the same functional consequences across cortical regions. Here, it is important to again consider graph theoretical results from the local PPC within the context of whole-brain connectivity. Earlier, it was discussed how between-network interactions are impaired in TBI, and this may be due partly to deficient functional long-range connectivity (Han et al., 2016) related to primary and secondary injury factors damaging long-distance fiber tracts (Sharp, Scott, & Leech, 2014). In light of long-range compromise, the current findings suggest that information transfer may not only occur, but may preferentially occur at a local level in TBI. Reduced between-network connectivity does not imply that information transfer does not exist or simply happens to

a lesser degree, but that it happens less efficaciously. Previous work in our lab has observed increased network *cliqueness* (quantified by the clustering coefficient) after TBI, which suggests that injury enhances communication between neighbors of a given node (Hillary, Rajtmajer, et al., 2014; Nakamura et al., 2009; Roy et al., 2017). As discussed in a recent review by Hillary and Grafman (2017), this phenomenon may reflect alternate, local pathways (or detours) through which node-to-node communication is achieved. Moreover, a hallmark cognitive deficit of DAI is reduced information processing speed, which may be a direct manifestation of reduced connection parsimony in TBI. Hence, hyperconnectivity within the local PPC network may reflect information integration through more inefficient, local channels in the face of damaged structural connectivity impeding larger-scale integration (Kuceyeski et al., 2016). It is critical to note here that by suggesting alternative information synthesis and consolidation processes in the brain, there is no proposition of functional reorganization, as the PPC remains indisputably heteromodal and a viable site of information transfer. Rather, a sort of functional bootstrapping appears to occur in TBI wherein there is a redistribution (global to local), versus reassignment, of functional network processing (Hillary, 2008; Olsen et al., 2015; Scheibel et al., 2011).

Local PPC Network Properties and Behavior

Results of the current study provide support for the special behavioral relevance of right PPC functionality in TBI; interestingly, however, there is evidence that different graph theory metrics of network integrity may reveal qualities of distinct behavioral features. In keeping with the idea that local PPC hyperconnectivity as a coping response to injury that reflects inefficient neural communication, the study observed

worse RBANS Digit Span performance with increasing right PPC connection strength in TBI. This finding is line with previous work that has found behaviorally detrimental correlates of increased functional synchronization in task-based fMRI data (Caeyenberghs et al., 2012; Hillary, Medaglia, Gates, Molenaar, & Good, 2014), although effects in the opposite direction have been reported as well (Bonnelle et al., 2011; Sharp et al., 2011). Inconsistencies in the literature may be due to the diverse study designs, connectivity measures, and behavioral paradigms employed. The latter two may be especially important considerations in view of the current study's additional observation that increased global efficiency was associated with faster reaction time in TBI.

Although strength and efficiency showed moderate positive correlation in the full sample, the study findings suggest that increased strength and global efficiency of the PPC do not confer the same behavioral consequences. Because right PPC strength was related to poorer simple (untimed) attentional performance and right PPC global efficiency was directly related to complex attentional processing speed, the findings are suggestive of a cost-efficiency trade-off. Although it was not directly tested in the current study, the proclivity towards balancing cost with efficiency has been well investigated as a characteristic feature of small-world networks such as the brain (Achard & Bullmore, 2007; Bassett & Bullmore, 2006; Kaiser & Hilgetag, 2006), and it is likely being observed here once again on a smaller scale. It was also the target of investigation in a recent study of TBI, which found that while cost was related to better untimed working memory performance, it was also associated with worse simple processing speed and speeded executive functioning (Roy et al., 2017). These results bear some similarity to

the current findings, which substantiate a cost-efficiency trade-off at local levels of network processing. Furthermore, the dissociation of network metrics and their behavioral correlates may potentially explain not only heterogeneity of cognitive sequelae within TBI samples, but also the marked intraindividual variability in cognitive test performance that has been observed in the general population.

Limitations, Future Directions, and Conclusions

Rapidly developing advanced connectivity methods are providing exciting new ways to map the human connectome, which has been an endeavor for well over a decade now. A delineation of whole-brain structure and function has been a major target of these methods, which have revealed critical aspects of brain organization and their relevance to behavior in normal and disrupted neurologic environments. However, any substantive understanding of whole-brain functionality requires recognition of the brain as a hierarchical entity with multiple points of systemic convergence that facilitate global network communication. The current study was an investigation of this local functional landscape to determine if the granularity afforded by such an approach could reveal additional insights into the nature of network plasticity in a disrupted neural system. In its attempt, the study faced significant challenges, briefly discussed below.

From a procedural standpoint, sample sizes were limited due to the difficulty in recruiting both individuals with TBI and appropriate controls, and limited information was available regarding the nature of individual injuries. Also because of the mixed nature of the sample, the availability of neuropsychological and other cognitive variables was limited. Importantly, to maximize sample size, individuals comprising a wide age range

and varying stages of recovery were incorporated into a single TBI group. It is well known that functional connectivity indices track with factors such as age and time post-injury, and the influence of such confounds cannot be discounted in the present work. However, age and time post-injury showed overall little relationship to connectivity metrics in this study, suggesting that the hemispheric and group differences observed are in some part independent of individual-specific characteristics. It should be noted that notwithstanding sample heterogeneity, two effects were striking and consistent with previous literature: increased connectivity strength in the TBI group, and support for a unique right-hemispheric contribution to network functioning after injury. Moreover, there was less variability in modular structure despite clinical heterogeneity in the TBI group, and an even stronger effect in this direction would be expected in a more homogeneous clinical sample. Thus, the pattern of results suggests that the study captured independent effects of brain injury, that is, neurologic sequelae that can be separated from premorbid, peritraumatic, or posttraumatic factors despite theoretically being modulated by them to some degree. The moderate-severe TBI literature has been riddled by inter-individual differences in personal and injury characteristics as well as treatment and management of chronic symptomatology, making the delineation of neuroplasticity after TBI quite challenging. In this light, the current study includes a fairly representative sample of individuals with head trauma, and highlights general injury-related neuroplastic mechanisms that may offer the most promise for intervention strategies.

Methodologically, the present work initially endeavored to utilize a modularity analysis with voxels in the PPC to parcellate it into smaller subregions than are given by

a priori atlas definitions or data-driven whole-brain parcellation schemes (e.g., clustering techniques or independent components analysis). While the Louvain algorithm appeared to perform well in detecting communities, it did not offer any further granularity than that afforded by other approaches. This is a known “resolution” problem of modularity optimization algorithms (Fortunato & Barthelemy, 2007), where, to use an example from geography, modularity on continents will result in modules of countries, modularity on countries will result in state modules, and so on. Modularity analyses did allow for investigation of interindividual variability, which produced interesting results between groups. However, given the custom scripts used in the current analyses, which involved specific coding procedures to examine graph theoretical properties of the PPC at the voxel level, the mapping of PPC modules onto anatomy could not be feasibly discerned.

Further research is needed to increase the resolution of connectivity analyses within heteromodal areas like the PPC, which may lead to several mini-connectomes within a larger brain mapping endeavor that is already underway by many groups. For example, Nicolini and Bifone (2016) have proposed a modification of popular modularity approach based on probability theory to improve detection of smaller communities and connector hubs, which may prove useful for the goals described here. Additionally, while many multi-modal structural/functional studies exist, the current study reveals a need to chart local connectivity patterns on anatomical subregions, particularly in the context of widespread structural disconnection seen in TBI. This could shed light on the specific changes in connectivity patterns within components of the PPC to complement the broader network-based alterations reported in the current work. A final note for

future direction involves the limited tools researchers currently have to study behavioral relationships with connectivity metrics. This is perhaps a more widespread problem in the literature than is appreciated, as available instruments measure quite broad cognitive constructs, a conceptual coarseness that stands in contrast to the more fine-grained nature of brain connectivity analyses, particularly when conducted at the voxel-level. Advances in cognitive neuroscience, which are targeting component cognitive processes of gross cognitive abilities, hold considerable promise in this regard.

Despite its limitations, the current work emphasizes the importance of considering brain connectivity at all levels, conjointly, to more fully elucidate functional changes after complex and catastrophic neurologic insult. In doing so, it reveals nuances of network connectivity that enrich narratives of network connectivity and plasticity. Focusing on the PPC, a functionally heterogeneous cortical area where high traffic between systems is thought to occur, the study provides evidence for localized hemispheric specialization that is consistent with what is observed at the global level, and that is preserved even in the context of major brain trauma. Furthermore, the up-regulation of PPC network connectivity observed in TBI offers refinements to previous conceptualizations of network alterations in TBI by suggesting potential changes in resource allocation. Importantly, however, it appears that these local changes have multiple implications for cognitive functioning that are likely a function of the need to balance functional resource utilization with sufficiently rapid communication between distinct cognitive networks. The extent to which a given individual with TBI can achieve this equilibrium may be a useful operationalization of neural recovery in TBI moving forward.

Appendix A.

"Self-referential" prompts during modified 2-back task

Experimental paradigm: n-back and self-referential cognition

- 10 blocks of 2-back condition, 10 trials per block
- 10 blocks of prompts for self-referential thinking interposed between task blocks

1. For two minutes, write down any thoughts that enter your mind. For each, indicate whether it refers to the past, present, or future.

2. Think about any skills or talents you have, big or small. Identify one, and describe how you would feel if you won an award for it.

3. Identify an important milestone in someone's life. How would it make them feel once they reached it, and what might be their next goal?

4. If you could eat anything, indicate what your next meal would include. Don't forget dessert.

5. If someone gave you a $10 budget for a day, where would you go and on what would you spend it?

6. Imagine that you are lost in an unfamiliar country and cannot speak the language. Where would you go for help?

7. What are two reasons why someone would portray themselves as older than they actually are?

8. If a person made a friend or family member angry, what could they do to remedy the situation?

9. How are you feeling right now? Pay attention to any emotions or body sensations and provide at least two adjectives about your current mental state.

10. Imagine that you are in a movie theater and another theater-goer will not stop talking. What do you say to this person, and how might they respond?

Appendix B.

Commented code for all graph theoretical analyses (construction of G_{PPC}, calculation of Louvain modularity, and calculations of G_{PPC} strength, centrality, and efficiency; R statistical software)

```
#MODULARITY-BASED ROI PARCELLATION OF FUNCTIONAL MRI DATA


#Authored by Arnab Roy, Ph.D., Bioengineering, SUNY Binghamton; Postdoctoral Fellow, Dept. of
Psychology, Penn State University-University Park

#Modified and commented by Umesh Venkatesan, M.S., Doctoral Candidate, Dept. of Psychology, Penn
State University-University Park


#Date created: 31 March 2016

#Last updated: 01 May 2017


#-------------------------------------------------------------------------------------------


#INTRODUCTION: PLEASE READ ! !


#Purpose of the program: This program proceeds in 5 steps per ROI (referred to here as "region of
focus," or ROF, as singular or agglomerated contiguous ROIs can be inputted). The general goals
are detection, visualization, and quantitative characterization of communities in a *single* ROF.
This is achieved through exploitation of the Louvain modularity algorithm in a voxelwise fashion.

#1. The first step counts the voxels in the ROF and assigns each voxel (defined by its MNIxyz
coordinates) a numerical ID. This results in a file in which the number of lines is equal to the
number of voxels contained within the ROF, and the line number of a given voxel indicates its ID.

#2. The second step creates a lattice network (inclusive of corners and edges) and calculates the
pearson (R) correlation (connectivity) between possible voxel pairs in the lattice and also the
p-value of this of correlation. A file with this information is then created. Note that only
correlation values surviving the p-threshold defined in the the inputs (see below) are included.

#3. The third step performs Louvain modularity using the igraph package in R. The resulting file
contains community assignments for each voxel in the ROF.

#4. The fourth step creates a labelled NIFTI image such that all voxels belonging to the same
community receive the same numerical label. This image can be used for spatial visualization of
communities in Freesurfer.

#5. The fifth step calculates a single time series for each community by averaging across the
time series for all voxels in that community per timepoint. The community time series are
outputted in a file, and each time series is prepended with the number of voxels in that
community and "Y" if that community size met the user-defined threshold or "N" if it did not.
```

```
#-----------------------------------------------------------------------------------------------

#-----------------------------------------------------------------------------------------------

#Purpose of the program: This program will produce 1 file per ROF, such that each line will
contain the ROF_id, and coordinate

#of a voxel that belongs to this ROF. Thus the number of lines of this file is equal to the
number of voxels that

#belongs to this ROF. The line number of a voxel in this file is equal to its ROF-id

#-----------------------------------------------------------------------------------------------


#Load the required packages


library("fmri")

library("psych")

library("MASS")

library("lsr")

library("igraph")

library("brainGraph")


#-----------------------------------------------------------------------------------------------


#Define the input parameters.

#USER DEFINITIONS REQUIRED ! !


#Para 1: A list of ROF masks as a binary images (.img or .nii).

P_binary_mask <-
c("./ROIs_Use/resampledfROI_LeftPPC_MNI.img","./ROIs_Use/resampledfROI_RightPPC_MNI.img")


#Para 2: Text labels for each ROF.

P_region <- c("Left_PPC","Right_PPC")


#Para 3: A list of the functional files in 4D nifti (one per subject).

P_functional_list <- c("./functional_files/tbi/long.up.1.003_time5.nii")
```

```
#Para 4: A list of grey-matter skeletons in 4D nifti (one per subject, must be 1:1 with Para 3,
same order).

P_structural_list <- c("./structural_files/tbi/resample_wc1cr_long.up.1.003_time5.nii")



#Para 5: Define the FDR-corrected threshold for correlations (connections, edges).

P_fdr_threshold <- 0.05



#Para 6: Define a community size threshold. Note that modularity will be performed without
respect to threshold, but the output will identify with "Y" or "N" the qualifying communities.

P_community_size_threshold <- 0



#Para 7: Define the grey-matter mask threshold (i.e., the value to be multiplied with the max
grey matter skeleton value). 0.6 is a defensible value (see Zalesky et. al, 2012, Human Brain
Mapping).

P_grey_threshold <- 0.6



#-------------------------------------------------------------------------------------------

#-------------------------------------------------------------------------------------------



#Prepare the structural data: c0 controls the grey-matter skeleton for each subject.



for(c0 in 1:length(P_structural_list))#For.c0.begins

        {

        #Read the inputted skeleton into 'greymask'.

         greymask <- read.NIFTI(P_structural_list[c0], level = 0.75,setmask=FALSE)

        #Extract quantitative data from 'greymask' into 'greymask_data'.

         greymask_data <- extract.data(greymask, what = "data")

        #Write the data as an ANALYZE file.


write.ANALYZE(array(greymask_data,c(greymask$dim[1],greymask$dim[2],greymask$dim[3],1)),file=past
e("./path/0_StructNIFTI_subj_",c0,sep=""))

        }#For.c0.ends



#Multiply the maximum value in the (subject-specific) mask by the threshold defined in inputs to
achieve a final grey-matter threshold to be used later for masking functional data.
```

```
grey_thr <- max(greymask_data)*P_grey_threshold


#Check output for each subject's threshold. Provided that each subject has the same maximum, this
value should be 153, which is 0.6 of the maximum value for UINT8 file types (255*0.6).

print(grey_thr)


#-------------------------------------------------------------------------------------------


#Note: Here begins the heart of the code: a large loop that performs steps 1-5 presented in the
introduction. Ends at line XXY.


#Prepare the ROF: c1 controls the binary ROF for each subject.


for(c1 in 1:length(P_binary_mask))#For.c1.begins

        {

        #Read the inputted ROF into 'mask'.

         mask <- read.ANALYZE(P_binary_mask[c1], level = 0.75,setmask=FALSE)

        #Extract quantitative data from 'mask' into 'mask_data'.

         mask_data <- extract.data(mask, what = "data")


        #Read the dimensions of the ROF.

         X_limit <- mask$dim[1] #Maximum number of voxels in x-direction

         Y_limit <- mask$dim[2] #Maximum number of voxels in y-direction

         Z_limit <- mask$dim[3] #Maximum number of voxels in z-direction


#-----------------------------------------------------------------------


        #Note the following loop is in the order (inner to outer) cx then cy and then cz. This
will count voxel coordinates in every direction and account for every combination of xyz
contained within the ROF (and within the grey-matter mask- see below).



        #The following lists will store the coordinates of the voxel that are part of the mask.
These are defined as empty vectors outside the loop so that data can be appended to them
iteratively inside the loop. This format is also found in object definitions further in the code.
```

```
x_list <- c()

y_list <- c()

z_list <- c()


for(cz in 1:Z_limit)#For.Bracket1.Begins

      {

       for(cy in 1:Y_limit)#For.Bracket2.Begins

             {

              for(cx in 1:X_limit)#For.Bracket3.Begins

                    {

                    #Mask ROF by subject's grey-matter mask. Binary value of a given
voxel in the ROF has to be 1, and the corresponding voxel in the grey-matter mask has to qualify
as grey matter (i.e., exceed threshold above).

                     if(mask_data[cx,cy,cz,1] > 0)

                           {

                            x_list <- c(x_list,cx)

                            y_list <- c(y_list,cy)

                            z_list <- c(z_list,cz)

                           }


                    }#For.Bracket3.Ends

             }#For.Bracket2.Ends

      }#For.Bracket1.Ends




#---------------------------------------------------------------------


       #Store the voxel IDs, one per voxel.


write(file=paste("./path/1_VOX_ID_",P_region[c1],sep=""),paste("VOX_id","x","y","z",sep="
"),ncol=100,append=FALSE)

       #For.VOX_id.begins, with the list of x-coordinates as reference (can have only as many
ROF-id's as x [or y or z] coordinates)
```

```
         for(VOX_id in 1:length(x_list))

                {

write(file=paste("./path/1_VOX_ID_",P_region[c1],sep=""),c(VOX_id,x_list[VOX_id],y_list[VOX_id],z
_list[VOX_id]),ncol=100,append=TRUE)

                }#For.VOX_id.ends


#This concludes the first step. Recall from intro: the program counts the voxels in the ROF and
assigns each voxel (defined by its MNIxyz coordinates) a numerical ID. This results in a file in
which the number of lines is equal to the number of voxels contained within the ROF, and the line
number of a given voxel indicates its ID.




#---------------------------------------------------------------------


        #Lattice construction: c2 controls the inputted functional files. Make the lattice
network for each functional file.


        for(c2 in 1:length(P_functional_list))#For.c2.begins

                {

                #Create the header of the lattice connectivity file for this subject


write(file=paste("./path/2_Lattice_subj_",c2,"_",P_region[c1],sep=""),paste("vertex_1","vertex_2"
,"weight","p_value"),ncol=100,append=FALSE)

                #Read the inputted functional file into 'f'.

                 f <- read.NIFTI(P_functional_list[c2], level = 0.75,setmask=FALSE)

                #Extract quantitative data from 'f' into 'f_data'.

                 f_data <- extract.data(f, what = "data")


                #Check if functional and structural images match in size

                 if(f$dim[1] != X_limit || f$dim[2] != Y_limit || f$dim[3] != Z_limit)

                       {

                        print("Arey yaar! Functional and structural image sizes do not match!");

                        quit("yes");

                       }
```

```
               #Store the correlation values for all lattice links (including those that fail
FDR).

                cor_list <- c()

               #Store the p values for all lattice links (including those that fail FDR).

                p_list   <- c()

               #Store each "sending" voxel (note, however, network will be undirected; pair 1,2
is same as 2,1).

                vertex_1 <- c()

               #Store each "receiving" voxel.

                vertex_2 <- c()



               #Time series extraction and correlation: c3 and c4 control functional signals in
individual voxels.

                for(c3 in 1:(length(x_list)-1)) #For.c3.begins

                      {

                       for(c4 in (c3+1):length(x_list)) #For.c4.begins

                              {

                              #Check if a given voxel and another voxel are neighbors!

                               if(abs(x_list[c3] - x_list[c4]) <= 1 &&  abs(y_list[c3] -
y_list[c4]) <= 1 &&  abs(z_list[c3] - z_list[c4]) <= 1)

                                     {

                                     #Extract from 'fdata' the first voxel's time series.

                                      signal_1 <-
f_data[x_list[c3],y_list[c3],z_list[c3],1:f$dim[4]]

                                     #Extract from 'fdata' the second voxel's time series.

                                      signal_2 <-
f_data[x_list[c4],y_list[c4],z_list[c4],1:f$dim[4]]



                                     #Calculate the correlation between time series 1 and 2. Add
this correlation to the existing list of correlations created in the loop.

                                      cor_list <- c(cor_list,cor(signal_1,signal_2))

                                     #Calculate the p_value of this correlation and add that to
the existing list of p_values.

                                      p_list <- c(p_list,cor.test(signal_1,signal_2)$p.value)



                                     #Store the voxel IDs of the neighboring voxels.
```

```
                                        vertex_1 <- c(vertex_1,c3)

                                        vertex_2 <- c(vertex_2,c4)


                                       }


                                  }#For.c4.ends

                            }#For.c3.ends


                       #Replace all NA p_values to 10000 and all NA correlations to 0.

                        p_list[is.na(p_list)] <- 10000

                        cor_list[is.na(p_list)] <- 0

#-----------------------------------------------------------------------


       #Lattice storage: c5 controls the lattice network output (on one row: two voxel IDs
[vertices], their correlation [edge], and the significance of that correlation [weight]).

       #FDR-correct the p_values and store the lattice network in a file.

        fdr_p_list <- p.adjust(p_list, method = "fdr")

        for(c5 in 1:length(fdr_p_list)) #For.c5.begins, with the length of p_list as reference
(can have only as many output entries as p-values)

                       {

                        if(fdr_p_list[c5] <= P_fdr_threshold)


       {write(file=paste("./path/2_Lattice_subj_",c2,"_",P_region[c1],sep=""),c(vertex_1[c5],ver
tex_2[c5],cor_list[c5],p_list[c5]),ncol=100,append=TRUE)}

                       }#For.c5.ends



       #This concludes the second step. Recall from intro: the program creates a lattice network
(inclusive of corners and edges) and calculates the pearson (R) correlation (connectivity)
between possible voxel pairs in the lattice and also the p-value of this of correlation. A file
with this information is then created. Note that only correlation values surviving the p-
threshold defined in the the inputs are included.




#-----------------------------------------------------------------------


       #Prepare for visualization: create a temporary NIFTI file where all voxels are set to 0.
```

```
         temp_NIFTI <- mask_data


        #Set all the voxels in this NIFTI to 0.
         for(cz in 1:Z_limit)#For.B1.Begins
               {
                for(cy in 1:Y_limit)#For.B2.Begins
                      {
                       for(cx in 1:X_limit)#For.B3.Begins
                             {
                              temp_NIFTI[cx,cy,cz,1] <- 0
                             }#For.B3.Ends
                      }#For.B2.Ends
               }#For.B1.Ends



#-------------------------------------------------------------------------


       #Run community detection on this network and also create a Nifti file that will have the
community numbers for the voxels


       g <- read.table(paste("./path/2_Lattice_subj_",c2,"_",P_region[c1],sep=""),header=TRUE)

       g1 <- graph.data.frame(abs(g),directed=FALSE)


       wc <- cluster_louvain(g1)

       voxel_membership <- wc$membership


       print( paste("subj_",c2,"_",P_region[c1]," Modularity = ",modularity(wc),sep="")) #print
out modularity value on the screen



write(file=paste("./path/3_Voxelmembership_subj_",c2,"_",P_region[c1],sep=""),paste("ROI_ID
Community_ID"),ncol=100,append=FALSE)


         print(c(length(voxel_membership),length(x_list)))
```

```
        #Print other graph metrics on screen and store in file.
         print(mean(betweenness(g1, v=V(g1), directed=FALSE, nobigint=FALSE, normalized=FALSE)))
         print(mean(betweenness(g1, v=V(g1), directed=FALSE, nobigint=FALSE, normalized=TRUE)))
         print(mean(degree(g1, v=V(g1), loops=FALSE, normalized=FALSE)))
         print(sd(degree(g1, v=V(g1), loops=FALSE, normalized=FALSE)))
         print(mean(degree(g1, v=V(g1), loops=FALSE, normalized=TRUE)))
         print(sd(degree(g1, v=V(g1), loops=FALSE, normalized=TRUE)))
         print(mean(strength(g1, vids=V(g1), loops=FALSE, weights=NULL)))
         print(sd(strength(g1, vids=V(g1), loops=FALSE, weights=NULL)))
         print(graph.efficiency(g1, type="global", weights=NULL, use.parallel=FALSE))
         print(graph.efficiency(g1, type="global", weights=NA, use.parallel=FALSE))

#-----------------------------------------------------------------------

        #Output community ID for each voxel: c6 controls the community assignments.
       for(c6 in 1:length(voxel_membership))#For.c6.begins
          {

write(file=paste("./path/3_Voxelmembership_subj_",c2,"_",P_region[c1],sep=""),paste(V(g1)$name[c6
],voxel_membership[c6],sep=" "),ncol=100,append=TRUE)

           ROF_ID_temp <- as.numeric(V(g1)$name[c6])

           temp_NIFTI[x_list[ROF_ID_temp],y_list[ROF_ID_temp],z_list[ROF_ID_temp],1] <-
voxel_membership[c6]

          }#For.c6.ends

        #This concludes the third step. Recall from intro: the program counts the voxels in the
ROF and assigns each voxel (defined by its MNIxyz coordinates) a numerical ID. This results in a
file in which the number of lines is equal to the number of voxels contained within the ROF, and
the line number of a given voxel indicates its ID.

        #Create a NIFTI file representing each voxel in terms of its community ID.
```

```
write.ANALYZE(array(temp_NIFTI,c(X_limit,Y_limit,Z_limit,1)),file=paste("./path/4_NIFTI_subj_",c2
,"_",P_region[c1],sep=""))


       #This concludes the fourth step. Recall from intro: the program creates a labelled NIFTI
image such that all voxels belonging to the same community receive the same numerical label. This
image can be used for spatial visualization of communities in Freesurfer.


#---------------------------------------------------------------------


       #Create one time series for each community identified: c7 controls which community we are
looking for and c8 scans through all voxels and selects those that belong to the c7 community.


write(file=paste("./path/5_Blobconnectivity_subj_",c2,"_",P_region[c1],sep=""),paste("#",date()),
ncol=100,append=FALSE)

        for(c7 in 1:length(unique(voxel_membership)))#For.c7.begins

              {

               avg_signal <- rep(0,f$dim[4]) #make a zero signal when this loop starts

               community_size <- length(voxel_membership[voxel_membership == c7])

                     for(c8 in 1:length(voxel_membership))#For.c8.begins

                            {

                             ROF_ID_temp <- c8 #fetch the voxels ROF-ID

                             if(voxel_membership[ROF_ID_temp] == c7)

                                    {avg_signal <- avg_signal +
f_data[x_list[ROF_ID_temp],y_list[ROF_ID_temp],z_list[ROF_ID_temp],1:f$dim[4]]/community_size}

                            }#For.c8.ends


       #Place a tag while storing the signal to indicate if this signal should be used later or
not. This is where "Y" and "N" are displayed in the output file to indicate that a community size
does or does not meet the size threshold as per the inputs.

        if(community_size < P_community_size_threshold)#If.community_size.begins

              {


write(file=paste("./path/5_Blobconnectivity_subj_",c2,"_",P_region[c1],sep=""),c(community_size,"
N",avg_signal),ncol=10000,append=TRUE)

      }#If.community_size.ends

              else

              {
```

```
write(file=paste("./path/5_Blobconnectivity_subj_",c2,"_",P_region[c1],sep=""),c(community_size,"
Y",avg_signal),ncol=10000,append=TRUE)

                }#If.community_size.ends


                }#For.c7.ends


#---------------------------------------------------------------------


        }#For.c2.ends


#---------------------------------------------------------------------


}#For.c1.ends
```

Appendix C.

Commented code for calculation of Jaccard and Sorensen similarity coefficients (R statistical software)

```
#JACCARD AND SORENSEN INTER-SUBJECT MODULAR SIMILARITY


#Authored by Arnab Roy, Ph.D., Bioengineering, SUNY Binghamton; Postdoctoral Fellow, Dept. of
Psychology, Penn State University-University Park

#Modified and commented by Umesh Venkatesan, M.S., Doctoral Candidate, Dept. of Psychology, Penn
State University-University Park


#Date created: 18 May 2016

#Last updated: 10 May 2017


#-------------------------------------------------------------------------------------------


#Purpose of the program: This program will calculate the Jaccard/Sorenson coefficient for 2
different labelings for a given set of voxels


#-------------------------------------------------------------------------------------------

#Load the required packages


library("MASS")

library("sqldf")

#-------------------------------------------------------------------------------------------




labelled_files <- c("./tbiOP/britne.up.1.002_time3/3_Voxelmembership_subj_1_Left_PPC",

"./subject1/3_Voxelmembership_subj_1_Left_PPC",

"./subject2/3_Voxelmembership_subj_1_Left_PPC")




#-------------------------------------------------------------------------------------------
```

```
#PLEASE NOTE THAT THROUGHOUT THIS CODE VOXELS WILL BE REFERRED TO IN TERMS OF ROI_ID


#c1 and c2 will control the pair of cases


for(c1 in 1:(length(labelled_files)-1))#for.c1.begins
   {
    for(c2 in (c1+1):length(labelled_files))#for.c2.begins
       {


        #read the labelled files
        case1 <- read.table(labelled_files[c1],header=TRUE)
        case2 <- read.table(labelled_files[c2],header=TRUE)


        #-------------------------------------------------------------------------------------


        #find the maximum labelled value for case1 and case2


        max_label_case1 <- max(case1$Community_ID)
        max_label_case2 <- max(case2$Community_ID)


        #-------------------------------------------------------------------------------------


        #create an empty overlap matrix
        #column1 <- Community for case1
        #column2 <- Community for case2
        #column3 <- Jaccard
        #column4 <- Sorenson
        overlap_matrix <- mat.or.vec((max_label_case1)*(max_label_case2),4)



        counter <- 1
```

```
#note community_id starts from 1

#compare each community from case-1 to case-2

for(c3 in 1:max_label_case1)#for.c3.begins

   {


    case_1_voxels <- subset(case1,case1$Community_ID == c3)$ROI_ID


    for(c4 in 1:max_label_case2)#for.c4.begins

      {


       case_2_voxels <- subset(case2,case2$Community_ID == c4)$ROI_ID


       intersection_size <- length(intersect(case_1_voxels,case_2_voxels))

       union_size <- length(union(case_1_voxels,case_2_voxels))


       #Jaccard

       J_average_int_by_union <- intersection_size/union_size


       #Sorenson

       S_average_int_by_union <-
2*intersection_size/(length(case_1_voxels)+length(case_2_voxels))




       overlap_matrix[counter,1] <- c3

       overlap_matrix[counter,2] <- c4

       overlap_matrix[counter,3] <- J_average_int_by_union

       overlap_matrix[counter,4] <- S_average_int_by_union


       counter <- counter + 1


      }#for.c4.ends

   }#for.c3.ends
```

```
        #-------------------------------------------------------------------------------------



        temp1 <- data.frame(overlap_matrix)


        colnames(temp1 ) <- c("case1_commid","case2_commid","J_int_by_union","S_int_by_union")


        summary1_j <- sqldf(paste("select case1_commid, max(J_int_by_union) max_int_by_union from
temp1  group by case1_commid",sep=" "))

        summary2_j <- sqldf(paste("select case2_commid, max(J_int_by_union) max_int_by_union from
temp1  group by case2_commid",sep=" "))


        mean_max_row_j <- mean(summary1_j$max_int_by_union)

        mean_max_col_j <- mean(summary2_j$max_int_by_union)


        summary1_s <- sqldf(paste("select case1_commid, max(S_int_by_union) max_int_by_union from
temp1  group by case1_commid",sep=" "))

        summary2_s <- sqldf(paste("select case2_commid, max(S_int_by_union) max_int_by_union from
temp1  group by case2_commid",sep=" "))


        mean_max_row_s <- mean(summary1_s$max_int_by_union)

        mean_max_col_s <- mean(summary2_s$max_int_by_union)






        print(c(c1,c2,(mean_max_row_j+mean_max_col_j)/2,(mean_max_row_s+mean_max_col_s)/2))



      }#for.c2.ends

   }#for.c1.ends
```

References

Achard, S., & Bullmore, E. (2007). Efficiency and cost of economical brain functional networks. *PLoS Comput Biol, 3*(2), e17. doi:10.1371/journal.pcbi.0030017

Alavash, M., Doebler, P., Holling, H., Thiel, C. M., & Giessing, C. (2015). Is functional integration of resting state brain networks an unspecific biomarker for working memory performance? *Neuroimage, 108*, 182-193. doi:10.1016/j.neuroimage.2014.12.046

Andrews-Hanna, J. R., Reidler, J. S., Sepulcre, J., Poulin, R., & Buckner, R. L. (2010). Functional-anatomic fractionation of the brain's default network. *Neuron, 65*(4), 550-562. doi:10.1016/j.neuron.2010.02.005

Andrews-Hanna, J. R., Saxe, R., & Yarkoni, T. (2014). Contributions of episodic retrieval and mentalizing to autobiographical thought: evidence from functional neuroimaging, resting-state connectivity, and fMRI meta-analyses. *Neuroimage, 91*, 324-335. doi:10.1016/j.neuroimage.2014.01.032

Arsalidou, M., Pascual-Leone, J., Johnson, J., Morris, D., & Taylor, M. J. (2013). A balancing act of the brain: activations and deactivations driven by cognitive load. *Brain Behav, 3*(3), 273-285. doi:10.1002/brb3.128

Bassett, D. S., & Bullmore, E. (2006). Small-world brain networks. *Neuroscientist, 12*(6), 512-523. doi:10.1177/1073858406293182

Behrmann, M., Geng, J. J., & Shomstein, S. (2004). Parietal cortex and attention. *Curr Opin Neurobiol, 14*(2), 212-217. doi:10.1016/j.conb.2004.03.012

Behzadi, Y., Restom, K., Liau, J., & Liu, T. T. (2007). A component based noise correction method (CompCor) for BOLD and perfusion based fMRI. *Neuroimage, 37*(1), 90-101. doi:10.1016/j.neuroimage.2007.04.042

Bernier, R. A., Roy, A., Venkatesan, U. M., Grossner, E. C., Brenner, E. K., & Hillary, F. G. (in press). Neural network segregation during task and rest in TBI: Examining the dedifferentiation hypothesis. *Frontiers in Neurology*.

Berryhill, M. E. (2012). Insights from neuropsychology: pinpointing the role of the posterior parietal cortex in episodic and working memory. *Front Integr Neurosci, 6*, 31. doi:10.3389/fnint.2012.00031

Bertolero, M. A., Yeo, B. T., & D'Esposito, M. (2015). The modular and integrative functional architecture of the human brain. *Proc Natl Acad Sci U S A, 112*(49), E6798-6807. doi:10.1073/pnas.1510619112

Biswal, B., Yetkin, F. Z., Haughton, V. M., & Hyde, J. S. (1995). Functional connectivity in the motor cortex of resting human brain using echo-planar MRI. *Magn Reson Med, 34*(4), 537-541.

Blondel, V. D., Guillaume, J., Lambiotte, R., & Lefebvre, E. (2008). Fast unfolding of communities in large networks. *Journal of Statistical Mechanics: Theory and Experient*(10), 10008-10012. doi:10.1088/1742-5468/2008/10/P10008

Bombardier, C. H., Fann, J. R., Temkin, N. R., Esselman, P. C., Barber, J., & Dikmen, S. S. (2010). Rates of major depressive disorder and clinical outcomes following traumatic brain injury. *JAMA, 303*(19), 1938-1945. doi:10.1001/jama.2010.599

Bonnelle, V., Ham, T. E., Leech, R., Kinnunen, K. M., Mehta, M. A., Greenwood, R. J., & Sharp, D. J. (2012). Salience network integrity predicts default mode network

function after traumatic brain injury. *Proc Natl Acad Sci U S A, 109*(12), 4690-4695. doi:10.1073/pnas.1113455109

Bonnelle, V., Leech, R., Kinnunen, K. M., Ham, T. E., Beckmann, C. F., De Boissezon, X., . . . Sharp, D. J. (2011). Default mode network connectivity predicts sustained attention deficits after traumatic brain injury. *J Neurosci, 31*(38), 13442-13451. doi:10.1523/jneurosci.1163-11.2011

Bray, S., Almas, R., Arnold, A. E., Iaria, G., & MacQueen, G. (2015). Intraparietal sulcus activity and functional connectivity supporting spatial working memory manipulation. *Cereb Cortex, 25*(5), 1252-1264. doi:10.1093/cercor/bht320

Buckner, R. L., Andrews-Hanna, J. R., & Schacter, D. L. (2008). The brain's default network: anatomy, function, and relevance to disease. *Ann N Y Acad Sci, 1124*, 1-38. doi:10.1196/annals.1440.011

Buckner, R. L., Sepulcre, J., Talukdar, T., Krienen, F. M., Liu, H., Hedden, T., . . . Johnson, K. A. (2009). Cortical hubs revealed by intrinsic functional connectivity: mapping, assessment of stability, and relation to Alzheimer's disease. *J Neurosci, 29*(6), 1860-1873. doi:10.1523/jneurosci.5062-08.2009

Buckner, R. L., Snyder, A. Z., Shannon, B. J., LaRossa, G., Sachs, R., Fotenos, A. F., . . . Mintun, M. A. (2005). Molecular, structural, and functional characterization of Alzheimer's disease: evidence for a relationship between default activity, amyloid, and memory. *J Neurosci, 25*(34), 7709-7717. doi:10.1523/jneurosci.2177-05.2005

Bullmore, E., & Sporns, O. (2009). Complex brain networks: graph theoretical analysis of structural and functional systems. *Nat Rev Neurosci, 10*(3), 186-198. doi:10.1038/nrn2575

Cabeza, R., Ciaramelli, E., Olson, I. R., & Moscovitch, M. (2008). The parietal cortex and episodic memory: an attentional account. *Nat Rev Neurosci, 9*(8), 613-625. doi:10.1038/nrn2459

Cabeza, R., Mangels, J., Nyberg, L., Habib, R., Houle, S., McIntosh, A. R., & Tulving, E. (1997). Brain regions differentially involved in remembering what and when: a PET study. *Neuron, 19*(4), 863-870.

Caeyenberghs, K., Leemans, A., Heitger, M. H., Leunissen, I., Dhollander, T., Sunaert, S., . . . Swinnen, S. P. (2012). Graph analysis of functional brain networks for cognitive control of action in traumatic brain injury. *Brain, 135*(Pt 4), 1293-1307. doi:10.1093/brain/aws048

Caeyenberghs, K., Verhelst, H., Clemente, A., & Wilson, P. H. (2016). Mapping the functional connectome in traumatic brain injury: What can graph metrics tell us? *Neuroimage*. doi:10.1016/j.neuroimage.2016.12.003

Cao, M., Wang, J. H., Dai, Z. J., Cao, X. Y., Jiang, L. L., Fan, F. M., . . . He, Y. (2014). Topological organization of the human brain functional connectome across the lifespan. *Dev Cogn Neurosci, 7*, 76-93. doi:10.1016/j.dcn.2013.11.004

Cappell, K. A., Gmeindl, L., & Reuter-Lorenz, P. A. (2010). Age differences in prefontal recruitment during verbal working memory maintenance depend on memory load. *Cortex, 46*(4), 462-473. doi:10.1016/j.cortex.2009.11.009

Caspers, S., Eickhoff, S. B., Geyer, S., Scheperjans, F., Mohlberg, H., Zilles, K., & Amunts, K. (2008). The human inferior parietal lobule in stereotaxic space. *Brain Struct Funct, 212*(6), 481-495. doi:10.1007/s00429-008-0195-z

Caspers, S., Eickhoff, S. B., Rick, T., von Kapri, A., Kuhlen, T., Huang, R., . . . Zilles, K. (2011). Probabilistic fibre tract analysis of cytoarchitectonically defined human inferior parietal lobule areas reveals similarities to macaques. *Neuroimage, 58*(2), 362-380. doi:10.1016/j.neuroimage.2011.06.027

Caspers, S., Geyer, S., Schleicher, A., Mohlberg, H., Amunts, K., & Zilles, K. (2006). The human inferior parietal cortex: cytoarchitectonic parcellation and interindividual variability. *Neuroimage, 33*(2), 430-448. doi:10.1016/j.neuroimage.2006.06.054

Caspers, S., Schleicher, A., Bacha-Trams, M., Palomero-Gallagher, N., Amunts, K., & Zilles, K. (2013). Organization of the human inferior parietal lobule based on receptor architectonics. *Cereb Cortex, 23*(3), 615-628. doi:10.1093/cercor/bhs048

Chang, L., Speck, O., Miller, E. N., Braun, J., Jovicich, J., Koch, C., . . . Ernst, T. (2001). Neural correlates of attention and working memory deficits in HIV patients. *Neurology, 57*(6), 1001-1007.

Chang, T. Y., Huang, K. L., Ho, M. Y., Ho, P. S., Chang, C. H., Liu, C. H., . . . Liu, H. L. (2016). Graph theoretical analysis of functional networks and its relationship to cognitive decline in patients with carotid stenosis. *J Cereb Blood Flow Metab, 36*(4), 808-818. doi:10.1177/0271678x15608390

Choi, H. J., Zilles, K., Mohlberg, H., Schleicher, A., Fink, G. R., Armstrong, E., & Amunts, K. (2006). Cytoarchitectonic identification and probabilistic mapping of two distinct areas within the anterior ventral bank of the human intraparietal sulcus. *J Comp Neurol, 495*(1), 53-69. doi:10.1002/cne.20849

Cole, M. W., Pathak, S., & Schneider, W. (2010). Identifying the brain's most globally connected regions. *Neuroimage, 49*(4), 3132-3148. doi:10.1016/j.neuroimage.2009.11.001

Corbetta, M., Patel, G., & Shulman, G. L. (2008). The reorienting system of the human brain: from environment to theory of mind. *Neuron, 58*(3), 306-324. doi:10.1016/j.neuron.2008.04.017

Corbetta, M., & Shulman, G. L. (2002). Control of goal-directed and stimulus-driven attention in the brain. *Nat Rev Neurosci, 3*(3), 201-215. doi:10.1038/nrn755

Dikmen, S. S., Bombardier, C. H., Machamer, J. E., Fann, J. R., & Temkin, N. R. (2004). Natural history of depression in traumatic brain injury. *Arch Phys Med Rehabil, 85*(9), 1457-1464.

Duncan, E. S., & Small, S. L. (2016). Increased Modularity of Resting State Networks Supports Improved Narrative Production in Aphasia Recovery. *Brain Connect, 6*(7), 524-529. doi:10.1089/brain.2016.0437

Dwyer, D. B., Harrison, B. J., Yucel, M., Whittle, S., Zalesky, A., Pantelis, C., . . . Fornito, A. (2014). Large-scale brain network dynamics supporting adolescent cognitive control. *J Neurosci, 34*(42), 14096-14107. doi:10.1523/jneurosci.1634-14.2014

Eickhoff, S. B., Stephan, K. E., Mohlberg, H., Grefkes, C., Fink, G. R., Amunts, K., & Zilles, K. (2005). A new SPM toolbox for combining probabilistic cytoarchitectonic maps and functional imaging data. *Neuroimage, 25*(4), 1325-1335. doi:10.1016/j.neuroimage.2004.12.034

Fagerholm, E. D., Hellyer, P. J., Scott, G., Leech, R., & Sharp, D. J. (2015). Disconnection of network hubs and cognitive impairment after traumatic brain injury. *Brain, 138*(Pt 6), 1696-1709. doi:10.1093/brain/awv075

Filley, C. M. (2011). White matter: beyond focal disconnection. *Neurol Clin, 29*(1), 81-97, viii. doi:10.1016/j.ncl.2010.10.003

Fortunato, S., & Barthelemy, M. (2007). Resolution limit in community detection. *Proc Natl Acad Sci U S A, 104*(1), 36-41. doi:10.1073/pnas.0605965104

Fox, M. D., Corbetta, M., Snyder, A. Z., Vincent, J. L., & Raichle, M. E. (2006). Spontaneous neuronal activity distinguishes human dorsal and ventral attention systems. *Proc Natl Acad Sci U S A, 103*(26), 10046-10051. doi:10.1073/pnas.0604187103

Fox, M. D., Snyder, A. Z., Vincent, J. L., Corbetta, M., Van Essen, D. C., & Raichle, M. E. (2005). The human brain is intrinsically organized into dynamic, anticorrelated functional networks. *Proc Natl Acad Sci U S A, 102*(27), 9673-9678. doi:10.1073/pnas.0504136102

Friston, K. J., Frith, C. D., Fletcher, P., Liddle, P. F., & Frackowiak, R. S. (1996). Functional topography: multidimensional scaling and functional connectivity in the brain. *Cereb Cortex, 6*(2), 156-164.

Gennarelli, T. A., & Graham, D. I. (1998). Neuropathology of the Head Injuries. *Semin Clin Neuropsychiatry, 3*(3), 160-175.

Grady, C. L., McIntosh, A. R., & Craik, F. I. (2005). Task-related activity in prefrontal cortex and its relation to recognition memory performance in young and old adults. *Neuropsychologia, 43*(10), 1466-1481. doi:10.1016/j.neuropsychologia.2004.12.016

Gregoriou, G. G., Borra, E., Matelli, M., & Luppino, G. (2006). Architectonic organization of the inferior parietal convexity of the macaque monkey. *J Comp Neurol, 496*(3), 422-451. doi:10.1002/cne.20933

Greicius, M. D., Krasnow, B., Reiss, A. L., & Menon, V. (2003). Functional connectivity in the resting brain: a network analysis of the default mode hypothesis. *Proc Natl Acad Sci U S A, 100*(1), 253-258. doi:10.1073/pnas.0135058100

Gusnard, D. A., & Raichle, M. E. (2001). Searching for a baseline: functional imaging and the resting human brain. *Nat Rev Neurosci, 2*(10), 685-694. doi:10.1038/35094500

Hampson, M., Driesen, N., Roth, J. K., Gore, J. C., & Constable, R. T. (2010). Functional connectivity between task-positive and task-negative brain areas and its relation to working memory performance. *Magn Reson Imaging, 28*(8), 1051-1057. doi:10.1016/j.mri.2010.03.021

Han, K., Chapman, S. B., & Krawczyk, D. C. (2016). Disrupted Intrinsic Connectivity among Default, Dorsal Attention, and Frontoparietal Control Networks in Individuals with Chronic Traumatic Brain Injury. *J Int Neuropsychol Soc, 22*(2), 263-279. doi:10.1017/s1355617715001393

Harris, N. G., Verley, D. R., Gutman, B. A., Thompson, P. M., Yeh, H. J., & Brown, J. A. (2016). Disconnection and hyper-connectivity underlie reorganization after TBI: A rodent functional connectomic analysis. *Exp Neurol, 277*, 124-138. doi:10.1016/j.expneurol.2015.12.020

Hayes, J. P., Bigler, E. D., & Verfaellie, M. (2016). Traumatic Brain Injury as a Disorder of Brain Connectivity. *J Int Neuropsychol Soc, 22*(2), 120-137. doi:10.1017/s1355617715000740

He, Y., Wang, J., Wang, L., Chen, Z. J., Yan, C., Yang, H., . . . Evans, A. C. (2009). Uncovering intrinsic modular organization of spontaneous brain activity in humans. *PLoS One, 4*(4), e5226. doi:10.1371/journal.pone.0005226

Hellyer, P. J., Scott, G., Shanahan, M., Sharp, D. J., & Leech, R. (2015). Cognitive Flexibility through Metastable Neural Dynamics Is Disrupted by Damage to the Structural Connectome. *J Neurosci, 35*(24), 9050-9063. doi:10.1523/jneurosci.4648-14.2015

Hillary, F. G. (2008). Neuroimaging of working memory dysfunction and the dilemma with brain reorganization hypotheses. *J Int Neuropsychol Soc, 14*(4), 526-534. doi:10.1017/s1355617708080788

Hillary, F. G., Genova, H. M., Chiaravalloti, N. D., Rypma, B., & DeLuca, J. (2006). Prefrontal modulation of working memory performance in brain injury and disease. *Hum Brain Mapp, 27*(11), 837-847. doi:10.1002/hbm.20226

Hillary, F. G., & Grafman, J. H. (2017). Injured Brains and Adaptive Networks: The Benefits and Costs of Hyperconnectivity. *Trends Cogn Sci, 21*(5), 385-401. doi:10.1016/j.tics.2017.03.003

Hillary, F. G., Medaglia, J. D., Gates, K. M., Molenaar, P. C., & Good, D. C. (2014). Examining network dynamics after traumatic brain injury using the extended unified SEM approach. *Brain Imaging Behav, 8*(3), 435-445. doi:10.1007/s11682-012-9205-0

Hillary, F. G., Rajtmajer, S. M., Roman, C., Medaglia, J. D., Slocomb, J., Good, D. C., & Wylie, G. R. (2014). The rich get richer: brain injury elicits hyperconnectivity in core subnetworks. *PLoS One, 9*(8). doi:10.1371/journal.pone.0104021

Hillary, F. G., Roman, C. A., Venkatesan, U., Rajtmajer, S. M., Bajo, R., & Castellanos, N. D. (2015). Hyperconnectivity is a fundamental response to neurological disruption. *Neuropsychology, 29*(1), 59-75. doi:10.1037/neu0000110

Hillary, F. G., Slocomb, J., Hills, E. C., Fitzpatrick, N. M., Medaglia, J. D., Wang, J., . . . Wylie, G. R. (2011). Changes in resting connectivity during recovery from severe traumatic brain injury. *Int J Psychophysiol, 82*(1), 115-123. doi:10.1016/j.ijpsycho.2011.03.011

Hoofien, D., Gilboa, A., Vakil, E., & Donovick, P. J. (2001). Traumatic brain injury (TBI) 10-20 years later: a comprehensive outcome study of psychiatric symptomatology, cognitive abilities and psychosocial functioning. *Brain Inj, 15*(3), 189-209. doi:10.1080/026990501300005659

Hutchinson, J. B., Uncapher, M. R., & Wagner, A. D. (2009). Posterior parietal cortex and episodic retrieval: convergent and divergent effects of attention and memory. *Learn Mem, 16*(6), 343-356. doi:10.1101/lm.919109

Igelstrom, K. M., & Graziano, M. S. (2017). The inferior parietal lobule and temporoparietal junction: A network perspective. *Neuropsychologia*. doi:10.1016/j.neuropsychologia.2017.01.001

Jaccard, P. (1912). The distribution of flora in the Alpine zone. *New Phytologist, 11*, 37-50. doi:10.1111/j.1469-8137.1912.tb05611.x

Jerde, T. A., Merriam, E. P., Riggall, A. C., Hedges, J. H., & Curtis, C. E. (2012). Prioritized maps of space in human frontoparietal cortex. *J Neurosci, 32*(48), 17382-17390. doi:10.1523/jneurosci.3810-12.2012

Jilka, S. R., Scott, G., Ham, T., Pickering, A., Bonnelle, V., Braga, R. M., . . . Sharp, D. J. (2014). Damage to the Salience Network and interactions with the Default Mode Network. *J Neurosci, 34*(33), 10798-10807. doi:10.1523/jneurosci.0518-14.2014

Kaiser, M., & Hilgetag, C. C. (2006). Nonoptimal component placement, but short processing paths, due to long-distance projections in neural systems. *PLoS Comput Biol, 2*(7), e95. doi:10.1371/journal.pcbi.0020095

Kelly, A. M., Uddin, L. Q., Biswal, B. B., Castellanos, F. X., & Milham, M. P. (2008). Competition between functional brain networks mediates behavioral variability. *Neuroimage, 39*(1), 527-537. doi:10.1016/j.neuroimage.2007.08.008

Kim, J., Parker, D., Whyte, J., Hart, T., Pluta, J., Ingalhalikar, M., . . . Verma, R. (2014). Disrupted structural connectome is associated with both psychometric and real-world neuropsychological impairment in diffuse traumatic brain injury. *J Int Neuropsychol Soc, 20*(9), 887-896. doi:10.1017/s1355617714000812

Kim, J., Whyte, J., Patel, S., Avants, B., Europa, E., Wang, J., . . . Detre, J. A. (2010). Resting cerebral blood flow alterations in chronic traumatic brain injury: an arterial spin labeling perfusion FMRI study. *J Neurotrauma, 27*(8), 1399-1411. doi:10.1089/neu.2009.1215

Kirchner, W. K. (1958). Age differences in short-term retention of rapidly changing information. *J Exp Psychol, 55*(4), 352-358.

Koponen, S., Taiminen, T., Portin, R., Himanen, L., Isoniemi, H., Heinonen, H., . . . Tenovuo, O. (2002). Axis I and II psychiatric disorders after traumatic brain injury: a 30-year follow-up study. *Am J Psychiatry, 159*(8), 1315-1321.

Kuceyeski, A., Shah, S., Dyke, J. P., Bickel, S., Abdelnour, F., Schiff, N. D., . . . Raj, A. (2016). The application of a mathematical model linking structural and functional connectomes in severe brain injury. *Neuroimage Clin, 11*, 635-647. doi:10.1016/j.nicl.2016.04.006

Latora, V., & Marchiori, M. (2001). Efficient behavior of small-world networks. *Phys Rev Lett, 87*(19), 198701. doi:10.1103/PhysRevLett.87.198701

Leech, R., Braga, R., & Sharp, D. J. (2012). Echoes of the brain within the posterior cingulate cortex. *J Neurosci, 32*(1), 215-222. doi:10.1523/jneurosci.3689-11.2012

Leech, R., Kamourieh, S., Beckmann, C. F., & Sharp, D. J. (2011). Fractionating the default mode network: distinct contributions of the ventral and dorsal posterior cingulate cortex to cognitive control. *J Neurosci, 31*(9), 3217-3224. doi:10.1523/jneurosci.5626-10.2011

Liang, P., Wang, Z., Yang, Y., & Li, K. (2012). Three subsystems of the inferior parietal cortex are differently affected in mild cognitive impairment. *J Alzheimers Dis, 30*(3), 475-487. doi:10.3233/jad-2012-111721

Maas, A. I., Stocchetti, N., & Bullock, R. (2008). Moderate and severe traumatic brain injury in adults. *Lancet Neurol, 7*(8), 728-741. doi:10.1016/s1474-4422(08)70164-9

Macaluso, E. (2010). Orienting of spatial attention and the interplay between the senses. *Cortex, 46*(3), 282-297. doi:10.1016/j.cortex.2009.05.010

Mattson, A. J., & Levin, H. S. (1990). Frontal lobe dysfunction following closed head injury. A review of the literature. *J Nerv Ment Dis, 178*(5), 282-291.

Mazaika, P. K., Hoeft, F., Glover, G. H., & Reiss, A. L. (2009). *Methods and software for fMRI analysis for clinical subjects*. Paper presented at the Hum Brain Mapp.

McAllister, T. W. (2008). Neurobehavioral sequelae of traumatic brain injury: evaluation and management. *World Psychiatry, 7*(1), 3-10.

McAllister, T. W. (2011). Neurobiological consequences of traumatic brain injury. *Dialogues Clin Neurosci, 13*(3), 287-300.

McDonald, B. C., Flashman, L. A., & Saykin, A. J. (2002). Executive dysfunction following traumatic brain injury: neural substrates and treatment strategies. *NeuroRehabilitation, 17*(4), 333-344.

McIntosh, T. K., Smith, D. H., Meaney, D. F., Kotapka, M. J., Gennarelli, T. A., & Graham, D. I. (1996). Neuropathological sequelae of traumatic brain injury: relationship to neurochemical and biomechanical mechanisms. *Lab Invest, 74*(2), 315-342.

Menon, V., & Uddin, L. Q. (2010). Saliency, switching, attention and control: a network model of insula function. *Brain Struct Funct, 214*(5-6), 655-667. doi:10.1007/s00429-010-0262-0

Meunier, D., Lambiotte, R., Fornito, A., Ersche, K. D., & Bullmore, E. T. (2009). Hierarchical modularity in human brain functional networks. *Front Neuroinform, 3*, 37. doi:10.3389/neuro.11.037.2009

Murphy, K., Birn, R. M., Handwerker, D. A., Jones, T. B., & Bandettini, P. A. (2009). The impact of global signal regression on resting state correlations: are anti-correlated networks introduced? *Neuroimage, 44*(3), 893-905. doi:10.1016/j.neuroimage.2008.09.036

Nakamura, T., Hillary, F. G., & Biswal, B. B. (2009). Resting network plasticity following brain injury. *PLoS One, 4*(12), e8220. doi:10.1371/journal.pone.0008220

Nicolini, C., & Bifone, A. (2016). Modular structure of brain functional networks: breaking the resolution limit by Surprise. *Sci Rep, 6*, 19250. doi:10.1038/srep19250

Niendam, T. A., Laird, A. R., Ray, K. L., Dean, Y. M., Glahn, D. C., & Carter, C. S. (2012). Meta-analytic evidence for a superordinate cognitive control network subserving diverse executive functions. *Cogn Affect Behav Neurosci, 12*(2), 241-268. doi:10.3758/s13415-011-0083-5

Olsen, A., Brunner, J. F., Indredavik Evensen, K. A., Finnanger, T. G., Vik, A., Skandsen, T., . . . Haberg, A. K. (2015). Altered Cognitive Control Activations after Moderate-to-Severe Traumatic Brain Injury and Their Relationship to Injury Severity and Everyday-Life Function. *Cereb Cortex, 25*(8), 2170-2180. doi:10.1093/cercor/bhu023

Palacios, E. M., Sala-Llonch, R., Junque, C., Roig, T., Tormos, J. M., Bargallo, N., & Vendrell, P. (2013). Resting-state functional magnetic resonance imaging activity and connectivity and cognitive outcome in traumatic brain injury. *JAMA Neurol, 70*(7), 845-851. doi:10.1001/jamaneurol.2013.38

Pandya, D. N., & Seltzer, B. (1982). Intrinsic connections and architectonics of posterior parietal cortex in the rhesus monkey. *J Comp Neurol, 204*(2), 196-210. doi:10.1002/cne.902040208

Power, J. D., Schlaggar, B. L., Lessov-Schlaggar, C. N., & Petersen, S. E. (2013). Evidence for hubs in human functional brain networks. *Neuron, 79*(4), 798-813. doi:10.1016/j.neuron.2013.07.035

Power, J. D., Schlaggar, B. L., & Petersen, S. E. (2015). Recent progress and outstanding issues in motion correction in resting state fMRI. *Neuroimage, 105*, 536-551. doi:10.1016/j.neuroimage.2014.10.044

Raichle, M. E., MacLeod, A. M., Snyder, A. Z., Powers, W. J., Gusnard, D. A., & Shulman, G. L. (2001). A default mode of brain function. *Proc Natl Acad Sci U S A, 98*(2), 676-682. doi:10.1073/pnas.98.2.676

Raichle, M. E., & Snyder, A. Z. (2007). A default mode of brain function: a brief history of an evolving idea. *Neuroimage, 37*(4), 1083-1090; discussion 1097-1089. doi:10.1016/j.neuroimage.2007.02.041

Rajtmajer, S. M., Roy, A., Albert, R., Molenaar, P. C., & Hillary, F. G. (2015). A voxelwise approach to determine consensus regions-of-interest for the study of brain network plasticity. *Front Neuroanat, 9*, 97. doi:10.3389/fnana.2015.00097

Rapoport, M. J. (2012). Depression following traumatic brain injury: epidemiology, risk factors and management. *CNS Drugs, 26*(2), 111-121. doi:10.2165/11599560-000000000-00000

Reuter-Lorenz, P. A., Jonides, J., Smith, E. E., Hartley, A., Miller, A., Marshuetz, C., & Koeppe, R. A. (2000). Age differences in the frontal lateralization of verbal and spatial working memory revealed by PET. *J Cogn Neurosci, 12*(1), 174-187.

Roy, A., Bernier, R. A., Wang, J., Benson, M., French, J. J., Jr., Good, D. C., & Hillary, F. G. (2017). The evolution of cost-efficiency in neural networks during recovery from traumatic brain injury. *PLoS One, 12*(4), e0170541. doi:10.1371/journal.pone.0170541

Rubinov, M., & Sporns, O. (2010). Complex network measures of brain connectivity: uses and interpretations. *Neuroimage, 52*(3), 1059-1069. doi:10.1016/j.neuroimage.2009.10.003

Sato, J. R., Biazoli, C. E., Jr., Salum, G. A., Gadelha, A., Crossley, N., Vieira, G., . . . Jackowski, A. P. (2016). Connectome hubs at resting state in children and adolescents: Reproducibility and psychopathological correlation. *Dev Cogn Neurosci, 20*, 2-11. doi:10.1016/j.dcn.2016.05.002

Scheibel, R. S., Newsome, M. R., Wilde, E. A., McClelland, M. M., Hanten, G., Krawczyk, D. C., . . . Levin, H. S. (2011). Brain activation during a social attribution task in adolescents with moderate to severe traumatic brain injury. *Soc Neurosci, 6*(5-6), 582-598. doi:10.1080/17470919.2011.588844

Scheperjans, F., Hermann, K., Eickhoff, S. B., Amunts, K., Schleicher, A., & Zilles, K. (2008). Observer-independent cytoarchitectonic mapping of the human superior parietal cortex. *Cereb Cortex, 18*(4), 846-867. doi:10.1093/cercor/bhm116

Seeley, W. W., Menon, V., Schatzberg, A. F., Keller, J., Glover, G. H., Kenna, H., . . . Greicius, M. D. (2007). Dissociable intrinsic connectivity networks for salience processing and executive control. *J Neurosci, 27*(9), 2349-2356. doi:10.1523/jneurosci.5587-06.2007

Seghier, M. L. (2013). The angular gyrus: multiple functions and multiple subdivisions. *Neuroscientist, 19*(1), 43-61. doi:10.1177/1073858412440596

Sharp, D. J., Beckmann, C. F., Greenwood, R., Kinnunen, K. M., Bonnelle, V., De Boissezon, X., . . . Leech, R. (2011). Default mode network functional and structural connectivity after traumatic brain injury. *Brain, 134*(Pt 8), 2233-2247. doi:10.1093/brain/awr175

Sharp, D. J., Scott, G., & Leech, R. (2014). Network dysfunction after traumatic brain injury. *Nat Rev Neurol, 10*(3), 156-166. doi:10.1038/nrneurol.2014.15

Shirer, W. R., Ryali, S., Rykhlevskaia, E., Menon, V., & Greicius, M. D. (2012). Decoding subject-driven cognitive states with whole-brain connectivity patterns. *Cereb Cortex, 22*(1), 158-165. doi:10.1093/cercor/bhr099

Shomstein, S. (2012). Cognitive functions of the posterior parietal cortex: top-down and bottom-up attentional control. *Front Integr Neurosci, 6*, 38. doi:10.3389/fnint.2012.00038

Shumskaya, E., van Gerven, M. A., Norris, D. G., Vos, P. E., & Kessels, R. P. (2017). Abnormal connectivity in the sensorimotor network predicts attention deficits in

traumatic brain injury. *Exp Brain Res, 235*(3), 799-807. doi:10.1007/s00221-016-4841-z

Sorensen, T. (1948). A method of establishing groups of equal amplitude in plant sociology based on similarity of species and its application to analyses of the vegetarian on Danish commons. *Kongelige Danske Videnskabernes Selskab, 5*, 1-13.

Sours, C., Raghavan, P., Medina, A. E., Roys, S., Jiang, L., Zhuo, J., & Gullapalli, R. P. (2017). Structural and Functional Integrity of the Intraparietal Sulcus in Moderate and Severe Traumatic Brain Injury. *J Neurotrauma, 34*(7), 1473-1481. doi:10.1089/neu.2016.4570

Speck, O., Ernst, T., Braun, J., Koch, C., Miller, E., & Chang, L. (2000). Gender differences in the functional organization of the brain for working memory. *Neuroreport, 11*(11), 2581-2585.

Sporns, O. (2011). The human connectome: a complex network. *Ann N Y Acad Sci, 1224*, 109-125. doi:10.1111/j.1749-6632.2010.05888.x

Sporns, O. (2013). Structure and function of complex brain networks. *Dialogues Clin Neurosci, 15*(3), 247-262.

Spreng, R. N. (2012). The fallacy of a "task-negative" network. *Front Psychol, 3*, 145. doi:10.3389/fpsyg.2012.00145

Spreng, R. N., & Schacter, D. L. (2012). Default network modulation and large-scale network interactivity in healthy young and old adults. *Cereb Cortex, 22*(11), 2610-2621. doi:10.1093/cercor/bhr339

Spreng, R. N., Sepulcre, J., Turner, G. R., Stevens, W. D., & Schacter, D. L. (2013). Intrinsic architecture underlying the relations among the default, dorsal attention, and frontoparietal control networks of the human brain. *J Cogn Neurosci, 25*(1), 74-86. doi:10.1162/jocn_a_00281

Spreng, R. N., Stevens, W. D., Chamberlain, J. P., Gilmore, A. W., & Schacter, D. L. (2010). Default network activity, coupled with the frontoparietal control network, supports goal-directed cognition. *Neuroimage, 53*(1), 303-317. doi:10.1016/j.neuroimage.2010.06.016

Szczepanski, S. M., Pinsk, M. A., Douglas, M. M., Kastner, S., & Saalmann, Y. B. (2013). Functional and structural architecture of the human dorsal frontoparietal attention network. *Proc Natl Acad Sci U S A, 110*(39), 15806-15811. doi:10.1073/pnas.1313903110

Tang, C. Y., Eaves, E., Dams-O'Connor, K., Ho, L., Leung, E., Wong, E., . . . Pasinetti, G. (2012). Diffuse Disconnectivity in tBi: a resting state fMri anD Dti stuDy. *Transl Neurosci, 3*(1), 9-14. doi:10.2478/s13380-012-0003-3

Team, R. C. (2013). R: A language and environment for statistical computing. Vienna, Austria: R Foundation fro Statistical Computing. Retrieved from http://www.R-project.org/

Teasdale, G., & Jennett, B. (1974). Assessment of coma and impaired consciousness. A practical scale. *Lancet, 2*(7872), 81-84.

Tomasi, D., & Volkow, N. D. (2010). Ultrafast method for mapping local functional connectivity hubs in the human brain. *Conf Proc IEEE Eng Med Biol Soc, 2010*, 4274-4277. doi:10.1109/iembs.2010.5626180

Tomasi, D., & Volkow, N. D. (2011). Functional connectivity hubs in the human brain. *Neuroimage, 57*(3), 908-917. doi:10.1016/j.neuroimage.2011.05.024

Triarhou, L. C. (2007). The Economo-Koskinas atlas revisited: cytoarchitectonics and functional context. *Stereotact Funct Neurosurg, 85*(5), 195-203. doi:10.1159/000103258

Uddin, L. Q., Kelly, A. M., Biswal, B. B., Castellanos, F. X., & Milham, M. P. (2009). Functional connectivity of default mode network components: correlation, anticorrelation, and causality. *Hum Brain Mapp, 30*(2), 625-637. doi:10.1002/hbm.20531

Uddin, L. Q., Supekar, K., Amin, H., Rykhlevskaia, E., Nguyen, D. A., Greicius, M. D., & Menon, V. (2010). Dissociable connectivity within human angular gyrus and intraparietal sulcus: evidence from functional and structural connectivity. *Cereb Cortex, 20*(11), 2636-2646. doi:10.1093/cercor/bhq011

van den Heuvel, M. P., Stam, C. J., Boersma, M., & Hulshoff Pol, H. E. (2008). Small-world and scale-free organization of voxel-based resting-state functional connectivity in the human brain. *Neuroimage, 43*(3), 528-539. doi:10.1016/j.neuroimage.2008.08.010

Van Dijk, K. R., Sabuncu, M. R., & Buckner, R. L. (2012). The influence of head motion on intrinsic functional connectivity MRI. *Neuroimage, 59*(1), 431-438. doi:10.1016/j.neuroimage.2011.07.044

Venkatesan, U. M., Dennis, N. A., & Hillary, F. G. (2015). Chronology and chronicity of altered resting-state functional connectivity after traumatic brain injury. *J Neurotrauma, 32*(4), 252-264. doi:10.1089/neu.2013.3318

Vincent, J. L., Kahn, I., Snyder, A. Z., Raichle, M. E., & Buckner, R. L. (2008). Evidence for a frontoparietal control system revealed by intrinsic functional connectivity. *J Neurophysiol, 100*(6), 3328-3342. doi:10.1152/jn.90355.2008

Vinette, S. A., & Bray, S. (2015). Variation in functional connectivity along anterior-to-posterior intraparietal sulcus, and relationship with age across late childhood and adolescence. *Dev Cogn Neurosci, 13*, 32-42. doi:10.1016/j.dcn.2015.04.004

Vossel, S., Geng, J. J., & Fink, G. R. (2014). Dorsal and ventral attention systems: distinct neural circuits but collaborative roles. *Neuroscientist, 20*(2), 150-159. doi:10.1177/1073858413494269

Wang, J., Zuo, X., & He, Y. (2010). Graph-based network analysis of resting-state functional MRI. *Front Syst Neurosci, 4*, 16. doi:10.3389/fnsys.2010.00016

Weissman, D. H., Roberts, K. C., Visscher, K. M., & Woldorff, M. G. (2006). The neural bases of momentary lapses in attention. *Nat Neurosci, 9*(7), 971-978. doi:10.1038/nn1727

Whitfield-Gabrieli, S., & Nieto-Castanon, A. (2012). Conn: a functional connectivity toolbox for correlated and anticorrelated brain networks. *Brain Connect, 2*(3), 125-141. doi:10.1089/brain.2012.0073

Yue, Q., Martin, R. C., Fischer-Baum, S., Ramos-Nunez, A. I., Ye, F., & Deem, M. W. (2017). Brain Modularity Mediates the Relation between Task Complexity and Performance. *J Cogn Neurosci*, 1-15. doi:10.1162/jocn_a_01142

Zhang, S., & Li, C. S. (2014). Functional clustering of the human inferior parietal lobule by whole-brain connectivity mapping of resting-state functional magnetic

resonance imaging signals. *Brain Connect, 4*(1), 53-69.

doi:10.1089/brain.2013.0191

Vita

Umesh M. Venkatesan

Education

1991-2004	Monroe Township Public Schools – Monroe Township, NJ
2004-2008	BA, Psychology, Johns Hopkins University – Baltimore, MD
2010-2014	MS, Psychology, Pennsylvania State University – University Park, PA

Selected Honors and Awards

2015	Research and Graduate Studies Office (RGSO) Dissertation Award *College of the Liberal Arts, Pennsylvania State University*
2015	Outstanding Publication by a Graduate Student Award *Department of Psychology, Pennsylvania State University*
2013	APA Division 40 Blue Ribbon Award for best student submission *APA Division 40 – Society for Clinical Neuropsychology*
2008	G. Stanley Hall Prize for Outstanding Achievement in Psychology *Department of Psychology, Johns Hopkins University*
2008	Phi Beta Kappa *Johns Hopkins University*

Publications

Venkatesan, U.M., Festa, E.K., Ott, B.R., & Heindel, W.C. (in press). What drives driving: differences in the relationship of visual search and sensory binding to driving performance between healthy aging and Alzheimer's disease. *Journal of the International Neuropsychological Society.*

Bernier, R.A., Roy, A., **Venkatesan, U.M.,** Grossner, E., Brenner, E., & Hillary, F.G. (2017). Examining neural network representation of task and rest following moderate and severe traumatic brain injury. *Frontiers in Neurology, 8,* 1-11. doi: 10.3389/fneur.2017.00297

Venkatesan, U.M., Dennis, N.A., & Hillary, F.G. (2015). Chronology and chronicity of altered resting-state functional connectivity after traumatic brain injury. *Journal of Neurotrauma, 32*(4), 252-264. doi: 10.1089/neu.2013.3318

Venkatesan, U.M., Rajtmajer, S.M., & Hillary, F.G. (2014). Connectivity modeling and neuroplasticity after traumatic brain injury. In J. Tracy, B. Hampstead, & K. Sathian (Eds.), *Plasticity of Cognition in Neurologic Disorders.* Oxford University Press.

Hillary, F.G., Roman, C.A, **Venkatesan, U.M.,** Bajo, R., Rajtmajer, S.M., Castellanos, N.D. (2014). Hyperconnectivity is a fundamental response to neurological disruption. *Neuropsychology, 29*(1), 59-75. doi: 10.1037/neu0000110

Medaglia, J.D., Ramanathan, D.M., **Venkatesan, U.M.,** & Hillary, F.G. (2011). The challenge of non-ergodicity in network neuroscience. *Network, 22*(1-4), 148-153. doi: 10.3109/ 09638237.2011.639604